A rheological law to describe powder agitation in a lab-scale paddle mixer: Shear band observation and dimensional analysis

Hayfa Boussoffara, Cendrine Gatumel, Blandine Malécot, Maxime Viau, Henri Berthiaux

Powder Technology 451 (2025) 120469

Contents lists available at ScienceDirect

Powder Technology

journal homepage: www.journals.elsevier.com/powder-technology

A rheological law to describe powder agitation in a lab-scale paddle mixer: Shear band observation and dimensional analysis

Hayfa Boussoffara [a,b], Cendrine Gatumel [a], Blandine Malécot [b], Maxime Viau [b], Henri Berthiaux [a,*]

[a] Université de Toulouse, centre RAPSODEE, UMR CNRS 5302, IMT Mines Albi, Albi, France
[b] Tetra Pak Powder Handling, Le May sur Èvre, France

HIGHLIGHTS

- Paddle-induced flows are characterised by the dense flow regime.
- Dimensional analysis and shear band observation are performed in a lab-scale mixer.
- A rheological law inspired from the *μ(I)-rheology* is developed for free-flowing powders.
- Hatano's three parameters equation adequately fits the experimental data.
- The parameters are found to be insensitive to particle size.

GRAPHICAL ABSTRACT

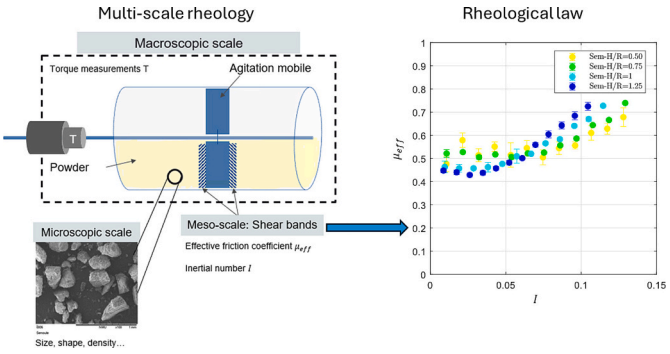

ARTICLE INFO

Keywords:
Powder
Rheology
Dense flow
Dimensional analysis
Shear band

ABSTRACT

This work adopts an in-system rheological approach to analyse powder flow behaviour in dense flows under mechanical agitation. For this purpose, an empirical law has been developed to assess powder rheology within a laboratory mixing setup, focusing on interactions between the paddles and the powder bed in dense flow. This model, is *an empirical* law, based on the μ(I)-rheology-like framework derived from dimensional analysis and shear band visualization. It reveals good predictive capabilities for powders of similar particle shapes but different sizes across various filling ratios. This approach addresses challenges in measuring complex powder parameters, such as the effective friction coefficient μ_{eff}, establishing a practical and easily applicable model that facilitates the scaling up of mixing processes and allows for better anticipation of forces exerted on the paddles. Comparisons with Hatano's equation showed a good fit with the rheological framework, particularly for deep powder beds. Better evaluation of the shear band width and reconsideration of normal stress assumptions may be the way forward to improve the accuracy of this μ(I)-rheology.

* Corresponding author.
E-mail address: henri.berthiaux@mines-albi.fr (H. Berthiaux).

https://doi.org/10.1016/j.powtec.2024.120469
Received 17 June 2024; Received in revised form 14 November 2024; Accepted 17 November 2024
Available online 21 November 2024

1. Introduction

Numerous industrial sectors, extending beyond the food industry, require the processing of granular materials at various stages of production. Powders can serve either as final products or as critical ingredients in a diverse array of goods. A key operation in powder handling is mixing, which is performed using a variety of technologies. Dry mixing allows for the homogenization of different types of powders [1] and is carried out in static, tumbling, convective mixers, etc.… In convective mixers, the powder bed is agitated by impellers, which forcibly displaces the powder in blocks from one region to another within the mixer's tank. In addition to convection, particles move in smaller groups due to shearing mechanisms. Impellers come in various shapes to achieve different mixing goals. Some resemble ribbons or screws, while others, like in Forberg-style mixer, features paddles [2,3]. Paddle mixers are usually composed of one or two shafts on which a certain number of paddles are mounted at specific rake angles. Powder flow within mixing equipment operating in batch mode is influenced by several factors, including operating conditions such as paddle agitation speed, filling ratio, and mixer geometry, as well as the powders' intrinsic and extrinsic properties. Therefore, understanding the powder flow behaviour when agitated mechanically in convective mixers is crucial.

Free-flowing powders, often perceived as easier to handle compared to cohesive powders due to weak inter-particle forces like Van der Waals or capillary forces, present challenges in predicting their flow behaviour due to potential particle segregation and agglomeration [4,5]. In a dynamic state, these powders primarily interact through frictional and collisional contacts, with forces that can vary depending on the shear rate.

The physical interactions of powders with the agitation mobile in mixers have been studied since the 60's, where Bagster and Bridgwater examined flow patterns near the surface around a horizontal stationary flat blade within a moving granular bed [6,7]. More recent research in a similar setup has shown interest in characterising powder flows around paddles using high-speed cameras and Discrete Element Method (DEM) [8–10]. These studies demonstrated the formation of recirculation zones in front of paddles and identified a velocity gradient within the moved powder bed [4,5,11]. They have also shown that the flow regime at the surface can be split into two types –rolling and cataracting– based on whether the Froude number is below or above one [12]. Through dimensional analysis, Legoix found that the in-system rheology within convective mixers can be described by a power law, constituting a process relationship, between the Froude number and the power number ($N_p = a.Fr^b$), where the proportionality coefficient a depends on the powder and on the filling ratio of the mixer, while the exponent b depends on the flow regime. This correlation, intended for scale-up purpose, does not account quantitively for the impact of powder characteristics [13]. Furthermore, the immersed regions, where frictional forces dominate, have often been overlooked due to the difficulty in obtaining insights into the flows taking place at such scale.

Research works have highlighted three regimes of powder flow depending on applied shear rates, with one intermediate regime exhibiting a liquid-like behaviour, referred to as a dense flow regime [14,15]. This regime, lying between the quasi-static and collisional flow regimes, involves complex interactions and fluctuating contact networks localised in a narrow region of about a dozen particle mean diameters where energy is dissipated by friction [16]. The dense flow regime is the most common regime in different industrial applications, including dry powder mixing. The localised area, referred to as the shear band, corresponds to a limited number of particles and can be said to be mesoscopic. Analysing flow at this scale may help to bridge the gap between individual particle interactions (microscopic scale) and the bulk flow behaviour (macroscopic scale). The thickness of the shear band tends to decrease slightly with increasing particle size and increase significantly with increasing confining stress. However, it was found to be independent from particle shape [17–22]. To better predict flow behaviour in agitation equipment like mixers, it is essential to take into consideration the shear band formation to build a multi-scale approach, therefore, linking the dynamics at a grain level to the overall structure of the flow.

To better account for particle characteristics, researchers have turned -during the last two decades- to a specific dimensionless number, the inertial number I ((Eq. (1)). It aims to describe the balance between interparticle momentum and energy dissipation, both of which governing the rheology of granular matters [14,23–25]:

$$I = \dot{\gamma} d \Big/ \sqrt{P/\rho_p} \tag{1}$$

Nevertheless, to address the discrete nature of granular materials, a constitutive law correlating I to the effective friction coefficient μ_{eff} has been established by numerical methods, to describe dense flow regimes $10^{-2} < I < 0.2$ [23] for various configurations, where the flow goes from free surface to confined [23]. This rheological law, referred to as *μ(I)-rheology*, was described empirically by Hatano [26] as:

$$\mu_{eff} = \mu_0 + bI^n \tag{2}$$

with μ_0 being the minimum dynamic friction coefficient as $I \to 0$, and b and n being constants specific to the material. The effective friction coefficient μ_{eff}, based on the Mohr-Coulomb definition, represents the ratio of the shear stress τ to the normal stress σ. In many studies, the normal stress has been approximated by hydrostatic pressure, though this assumption may be less accurate for thicker layers of material. For example, in dam-break scenarios or real landslides, the initially released mass may be substantial, affecting stress distributions [14,27–30]. Therefore, the dynamic pressure ought to be taken into account during the flow initiation. In the framework of this study, the flow initiation (the start-up of the mixer) is excluded and only the stationary regime is studied. Furthermore, in dense flows, particle interactions are dominated by contact forces, and dynamic pressure might have an insignificant impact.

The *μ(I)-rheology* has been extensively studied in planar shear configurations, where parameters are easily controllable and measurable, and stress distribution remains uniform within the sheared layer. At low shear rates, μ_{eff} remains constant, indicating a shear-independent behaviour of the powder, mainly governed by frictional forces. Beyond a certain value of I, μ_{eff} starts increasing rapidly with I, marking the threshold at which the flow becomes shear-dependant. Recent research using a laboratory vertical bladed mixer has shown, however, that μ_{eff} more accurately represents flow behaviour in deep powder beds compared to shallow ones [31].

This work aims to develop a rheological law based on the well-known μ(I)-rheology, to study and predict powder flow behaviour in immersed area within a laboratory mixing set-up, depicted in Fig. 1, following a dimensional analysis approach. The objective is then to assess the capability of μ(I)-rheology to predict flow behaviour for any type of convective mixer. This approach aims to provide a framework for comprehensively analysing powder flows under mechanical agitation, thereby aiding in the optimisation of mixing efficiency and the sustainability of processing operations. Ultimately, the goal is to develop scalable process relationships that will enable the transition of the mixing process in convective paddle mixers from laboratory to industrial scale.

The article is structured as follows: Section 2 details the materials and methods, including powder characteristics and the lab-scale mixing set-up. Section 3 presents the results and discussions, starting with the study of paddle-induced flows, followed by the development of a rheological law μ(I)-rheology through dimensional analysis, and concluding with the assessment of this law for two free-flowing powders – semolina and couscous. Finally, Section 4 provides the conclusions and suggests potential directions for future research.

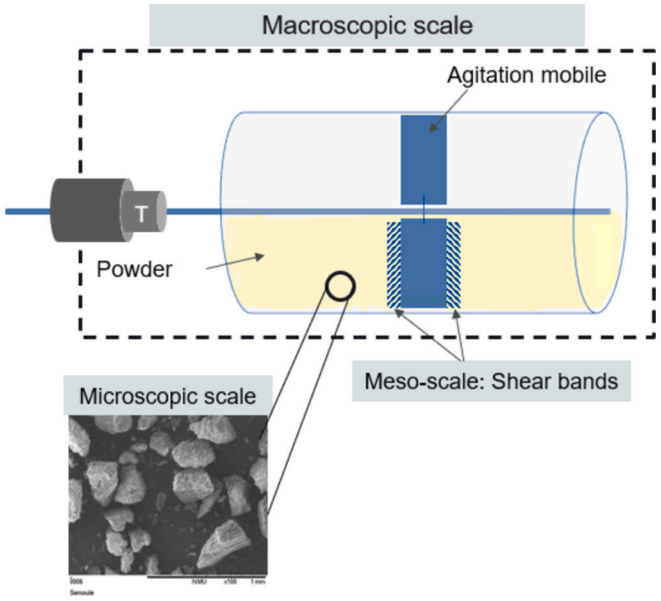

Fig. 1. Definition of macro, *meso*, and micro-scales within the laboratory set-up "C-lab mixer": Macro-scale represents the in-system scale; meso-scale refers to clusters of particles where friction occurs, and micro-scale denotes the scale of individual particles.

2. Materials and methods

2.1. Powder characteristics

In this work, the behaviour of two free-flowing powders under mechanical agitation is examined: fine semolina (Panzani®) and fine couscous (En Cuisine®). Both powders are stable under various conditions (temperature, moisture…) and offer uniformly sized particles of similar chemical composition.

Particle morphology, observed using a Scanning Electron Microscope (SEM) TM3030Plus (Hitachi®, Japan), is presented in Fig. 2. SEM images of semolina reveal irregularly shaped particles with relatively sharp edges and a rough surface. However, couscous particles, are roughly rounded with less pronounced surface irregularities.

Table 1 illustrates the measured properties of semolina and couscous. Mean particle diameter d_{50} was determined using a LASER diffraction with a Mastersizer3000 (Malvern Panalytical, Malvern®, UK). Bulk density ρ_b was measured using the SVM22 tapped density tester (Erweka®, Germany), while the particle density ρ_p was measured using an Accupyc® 1340 helium pycnometer (Micromeritics®, Mérignac, France). Carr Index CI%, indicating the ratio between the untapped and tapped powder densities, is calculated to assess the flowability of the powders. A CI% below 15 % implies that the powder is free-flowing. φ represents the maximum compacity of the powder bed and is defined as the ratio between ρ_b and ρ_p.

2.2. Lab-scale mixing set-up "C-lab mixer"

A cylindrical tank mechanically agitated, referred to as the C-lab mixer, that has been designed to carry out the thesis work of Legoix [13] is used in this work. The C-lab mixer consists in a transparent vessel made from polymethylmethacrylate (PMMA) of approximately 9 mm width and an effective capacity of around 8.85 l, thereby allowing flow visualization during agitation. As depicted in Fig. 3, the mixer is fitted with one shaft, sustained by two bearing bushes, supporting a row of four straight rectangular stainless-steel paddles, each set at 90°. The four paddles form a single agitation mobile as they cut through the same region of the powder bed. The configuration adapted for the tests of this framework is detailed in Fig. 3.b. The paddle length L_p is 3 mm shorter than the tank radius R, making a minimal gap sufficient to prevent particle blockage between the paddle tips and the tank wall. Given this small gap, L_p is assumed to be approximately equal to R.

The C-lab mixer is equipped with a torquemeter mounted on the

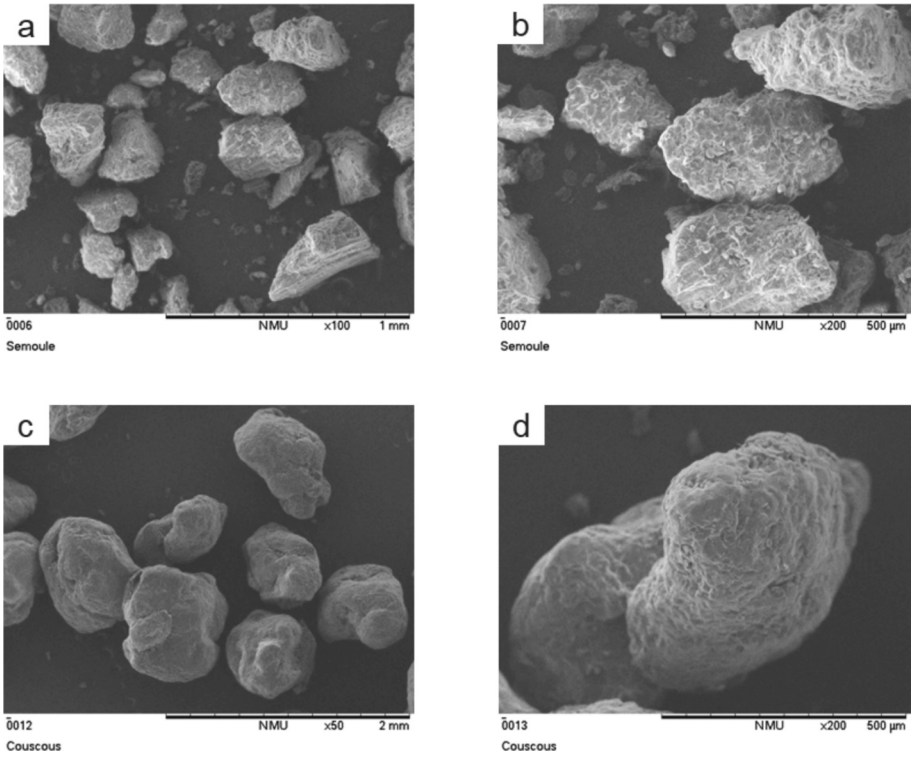

Fig. 2. SEM pictures of semolina (a. X100 and b. X200) and couscous (c. X50 and d.X200).

Table 1
Measured characteristic of semolina and couscous.

Powder	d_{10} (μm)	d_{50} (μm)	d_{90} (μm)	ρ_b ($kg.m^{-3}$)	ρ_p ($kg.m^{-3}$)	CI%	φ
Semolina	180	309	482	770	1438	5.8	0.53
Couscous	718	1005	1495	854	1591	5.3	0.57

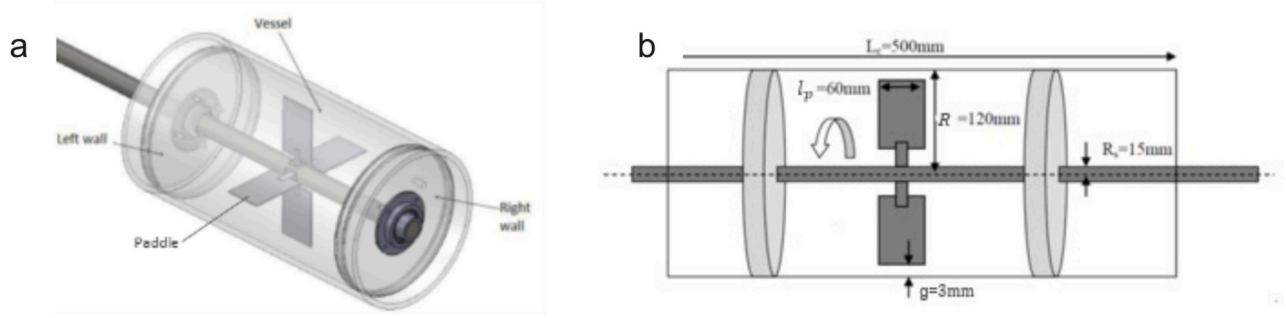

Fig. 3. C-lab mixer a. Overall drawing showing the blade assembly, and b. Frontal view detailing the dimensions of the mixer components.

shaft to measure the mechanical torque. The torquemeter has an accuracy of 0.25 %, applicable over the maximum measurement range of 10 N.m. The motor can operate within a rotational speed range spanning from 2 to 20 rad.s^{-1} thanks to reduction gearbox. A LabVIEW® interface controls paddle speed and records torque data, sampling every 0.02 s. The speed, torque measurements, powder mass, room temperature, and moisture percentage are logged into a spreadsheet for analysis.

2.2.1. Rheological measurements

The central parameter in this work is the torque which is a descriptor of the systems agitated by a rotating mobile. In practice, the recommended mixer speed is that which allows a balance to be achieved between inertia forces associated with the rotating mobile and the forces of gravity, ideally resulting in a Froude number *Fr* equal to 1. In the present work, the Froude number is calculated through:

$$Fr = \frac{L_p \times \omega^2}{g} \tag{3}$$

ω represents the angular speed setpoint ($rad.s^{-1}$), L_p the paddle length (m) and g the gravitational acceleration ($m.s^{-2}$).

To explore a wide range of operating conditions, various speeds and filling ratios were investigated in our study. Each test campaign begins with a one-hour preheating procedure for all mixers. During the initial minutes of preheating, torque measurements decrease due to the heating of bearing seals, which reduces frictional resistance and facilitates easier shaft rotation. As preheating continues, the mixer reaches its optimal operating temperature, stabilizing torque measurements. After preheating, the mixer tank is filled to achieve the desired filling level, and the powder bed surface is flattened to ensure consistent initial conditions before recording torque measurements. The filling ratio H/R is chosen based on the radius R, with H the maximum height of the powder bed at the centre of the tank. This linear filling ratio is derived from the volumetric filling ratio f% as explained in (Eq. (4)) and (Eq. (5)):

$$f\% = \frac{V_p}{V_{tank}} * 100 = \frac{m_p}{\rho_b V_{tank}} * 100 \tag{4}$$

$$f\% = \frac{H.\pi.H_{tank}2}{H_{tank}.\pi.R2} * 100 = \frac{1}{2}.\frac{H}{R} * 100 \tag{5}$$

Agitation and on-load torque T_L measurements begin simultaneously for each speed increment. Once the stationary regime is achieved, identified through signal visualization, agitation continues for an additional two minutes. Before each speed increase, the paddles are returned to their initial inclination, and the powder surface is levelled. Upon completing torque measurements for a given filling ratio, the mixer is emptied, and idle torque T_0 measurements are recorded at the tested speeds. The experimental protocol is summarised in Fig. 4. Tests are

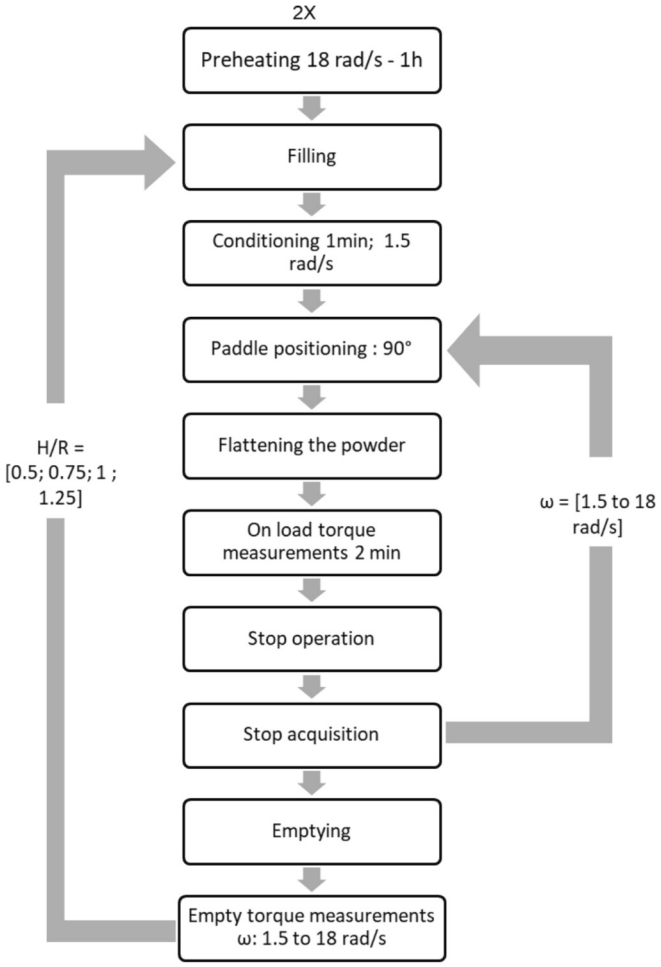

Fig. 4. Protocol for torque measurements carried out in the C-lab mixer with semolina and couscous for four filling ratios H/R and twelve rotational speeds ω.

conducted in duplicate for each angular speed and filling ratio to ensure the robustness and reliability of the results. Torque measurements are then processed and the useful time-averaged torque T is calculated following (Eq. (6)). The average of the time-averaged torques from both tests is presented, with standard deviation quantifying the associated error.

$$T = T_L - T_0 \tag{6}$$

2.2.2. Shear band observation

The mesoscopic scale is an intermediate size, that focuses on the interactions between clusters of particles and how these interactions influence the overall behaviour of the granular material. Often termed shear bands, this scale corresponds to narrow regions where particles experience localised rearrangement due to shear deformation induced by paddle movement. Shear bands typically exhibit a width of a few dozen particles [16,32].

To visualize the speed gradient near paddles and assess the thickness of the shear bands, a powder tracer technique was employed. This technique consists in colouring the same tested powder by impregnating it with an iodine solution [33]. The iodine will bind to the particles, which will become blackish. Initially, the semolina was coloured by spraying approximately 25 % of its mass with iodine solution (Bétadine®) while stirring. The powder is then laid out in fine layers to dry completely. However, colouring caused some semolina particles to form aggregates, necessitating a grinding step. The coloured semolina is subsequently sieved to achieve the same initial particle size distribution as the non-coloured semolina.

Once the coloured semolina is ready, shear band visualization is performed. About one-sixth of the total mass of black semolina is placed in the centre of the mixer using a quarter disc, allowing the powder to be poured in gradually using a fine funnel. The rest of the tank is filled with non-coloured semolina, as depicted in Fig. 5. The level of the powder bed is then flattened to obtain the same bed height throughout the tank. The quarter discs are then carefully removed to avoid jerky movements. The test was carried out with semolina in the C-lab mixer for 2 filling ratios, 0.75 and 1, and 3 speeds, 3, 6 and 15 rad/s, corresponding to Froude numbers of 0.1, 0.4 and 2.6.

The shear bands are then captured by a camera (Nikon®, Tokyo, Japan), with images taken by the Vic snap® software every minute for the initial five minutes and every 15 min thereafter. The shear band thickness considered is that measured after two minutes of agitation, corresponding to the mixing time used in our experiments. However, for a deeper understanding of its temporal evolution, images were taken over a longer duration.

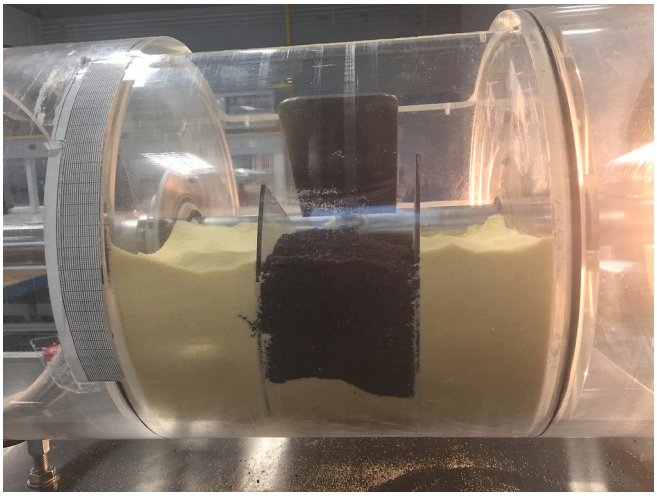

Fig. 5. Tracer initial position in the C-lab mixer.

3. Results and discussions

3.1. Paddle induced flows

3.1.1. Mesoscopic scale

The visualization of shear bands on both sides of the paddles during powder agitation in the C-lab mixer revealed four zones, as depicted in Fig. 6:

- Zone I is where the paddles pass, and the convection mechanism prevails.
- Zone II is where the particles are projected in avalanches, which are well visible during the rolling regime.
- Zone III is relatively immobile, with only the diffusion mechanism taking place.
- Zone IV is characterised by a velocity gradient and localised shear. This zone contains the shear band where the friction flow appears. The width W of the band is determined as shown in Fig. 6.

These observations are consistent with findings in the literature [16], where it has been demonstrated that in the zone directly above the intruder, particles exhibit a velocity close to that of the intruder (zone I). This reference also illustrates the existence of shear zones from both sides of the intruder (zone IV), where the particles tend to rearrange, and friction forces predominate. The flow within these shear zones is sustained throughout the entire agitation process by the consistent frequency of paddle passes through the powder bed. Another observation aligning with Lehuen's work is the void that appears behind the passage of the paddle, as shown in Fig. 7, particularly noticeable at relatively low speeds as the void is quickly filled by the passage of the following paddle at high speeds. The friction between individual particles within the shear bands, representing the mesoscopic scale differs from the "bulk" friction coefficient of the whole powder, which is of macroscopic nature. The shear band width W corresponds to the width of the coloured region at the bottom of the tank, extending from the lateral edges of the blade where a velocity gradient is observed, as shown in Fig. 6. W is measured at the bottom to focus on shearing mechanisms, as nearer to the surface, avalanches disturb the powder bed state, creating a diffusion of particles. Tests are carried out in duplicate.

The experiments with coloured semolina to evaluate the evolution of the shear band width W over time were carried out for three angular

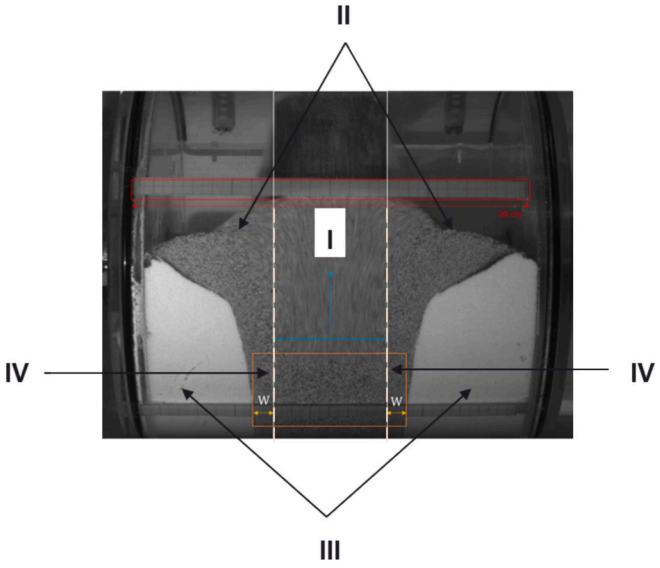

Fig. 6. Observation of four flow zones during agitation in the C-lab mixer and measurement of the shear band width W, corresponding to the coloured region width extending from the lateral edges of the paddle.

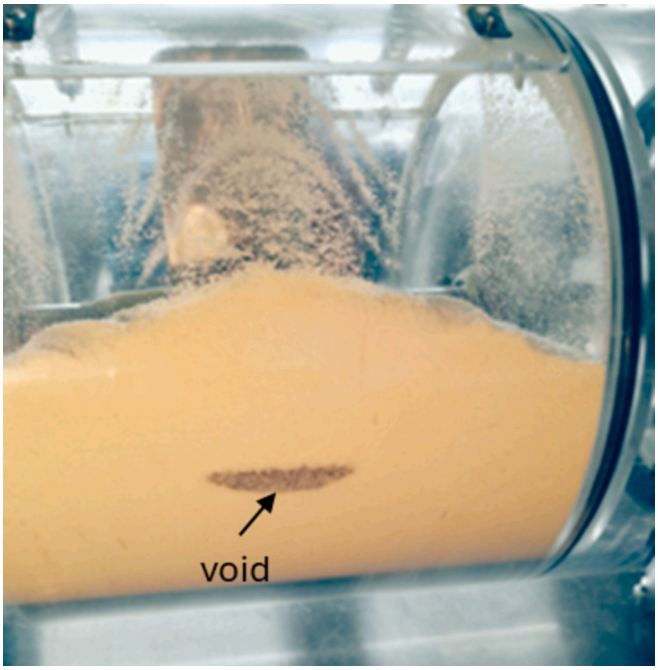

Fig. 7. Void appearance behind the paddle during agitation in the C-lab mixer.

speeds ω (3, 6, and 15 rad.s^{-1}) and two filling ratios $\frac{H}{R}$ (0.75 and 1), as illustrated in Fig. 8. W is found to be higher for higher angular speeds, at a same filling ratio. Additionally, it increases gradually during the initial 5 min of agitation, followed by a slow widening.

A choice has been made to work with the average width at 6 rad.s^{-1} corresponding to $Fr = 0.44$. This choice aligns with both the duration of the conducted tests and the industrial applications, it corresponds effectively to the dense regime under investigation ($Fr < 1$). A width W of around 1 cm will therefore be considered. It may be linked with the d_{50} of semolina (308 μm) and the number of particles involved in the shear band k through:

$$W = k \times d_{50} \quad (7)$$

In the present case, k equals approximately 30 semolina particles.

In this work, the shear band thickness is considered to be the same across all filling ratios, although it has been found to slightly decrease with increasing bed pressure according to Fig. 8. Additionally, the particle size and shape are two factors slightly impacting the shear band thickness according to the literature. However, the order of magnitude is always around a few dozen particles [17,20,32]. Given the complexity of conducting this type of tests to visualize the shear band, tests were limited to those with semolina and k is considered the same for both tested powders. The width W of shear bands during couscous agitation will therefore be considered equal to 3 cm.

Additionally, given the narrow gap between the tip of the paddle and the wall of the mixer tank, shear bands are considered to form solely along the paddle sides rather than at the front, due to limited space. The impact of wall friction was deemed negligible for our experimental conditions. Therefore, the analysis focuses on the shear behaviour taking place primarily on the sides of the paddle, where it is expected to have the most significant influence on the powder flow dynamics.

Observations indicate that the flow in the shear band region shows liquid-like behaviour, with particles sliding past each other continuously. This aligns with the dense flow regime description, which is the primary focus of our study.

3.1.2. Macroscopic scale

Torque measurements conducted in the C-lab mixer, aim to explore the in-system rheology. At a macroscopic scale, it represents the resistance of the powder bed to the mechanical action of the impeller, forced to maintain a constant angular speed. The mean of useful time-averaged torque T obtained from two repetitions with semolina for four linear filling ratios $\frac{H}{R}$ and twelve angular speeds ω is illustrated in Fig. 9.

Based on the Froude number Fr, calculated following (Eq. (3)), two regimes were identified by Legoix in the C-lab mixer, which are the rolling regime when $Fr < 1$ and the cataracting regime when $Fr > 1$ [12].

For $Fr < 1$, i.e. a rotational speed smaller than 9 rad.s^{-1}, the useful torque increases with increasing filling ratios, as expected, given that displacing a higher mass of a free-flowing powder requires a greater shear force. Across different rotational speeds, the torque remains relatively constant. In this rolling regime, gravity predominates over the centrifugal forces, prompting the powder to follow the paddle movement. When the paddle reaches a vertical position, it cascades down in avalanches. The constant torque profile may be attributed to the

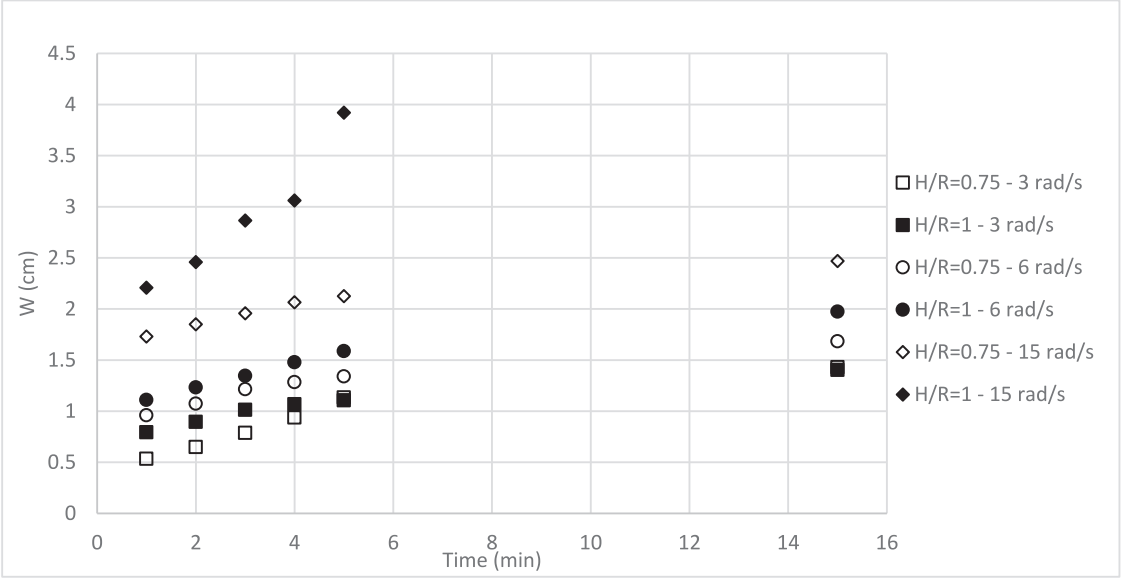

Fig. 8. Variations in the evolution of shear band width over time of semolina agitation for two filling ratios $H/R = 0.75$ and $H/R = 1$ across three different angular speeds ω = [3 rad.s-1, 6 rad.s-1, 15 rad.s-1].

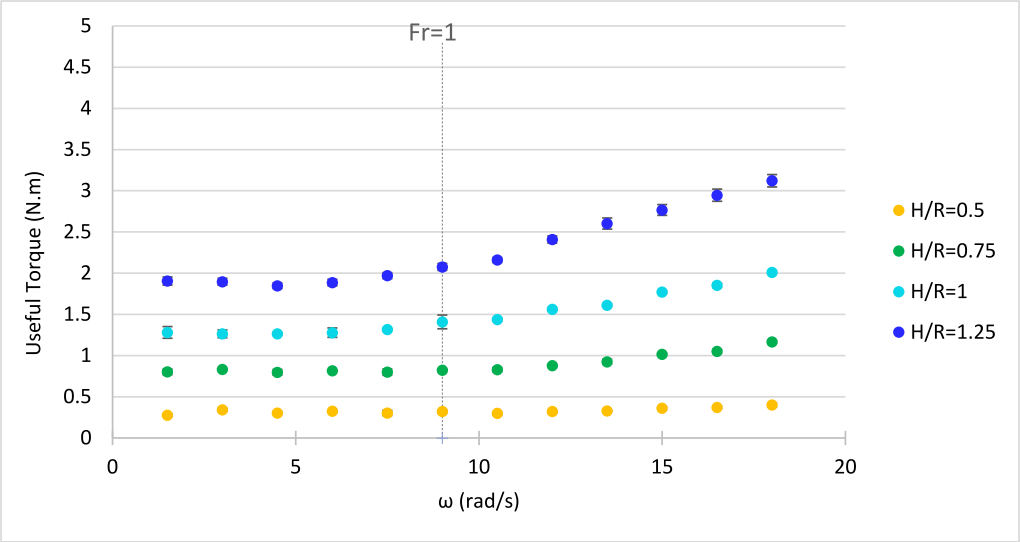

Fig. 9. Evolution of T as a function of ω for semolina in the C-lab mixer for increasing H/R (bottom to top) illustrating a shift in the behaviour once Fr exceeds 1, marked by a change from a rolling to a cataracting regime based on Fr.

resistance of the powder bed to paddle movement, which remains the same regardless of rotational speed due to the enduring contact between the powder and the paddle.

Once $Fr > 1$, a notable rise in torque is observed, demonstrating a shift in flow regimes from rolling to cataracting. At those high speeds, the powder is expelled on either side of the blades, creating a clearance zone that follows their movement. During the cataracting regime, the particles are no longer in permanent contact with the paddles as they are constantly projected in the air following the same trajectory of that of the paddles. At high filling ratios and rotational speeds, the gain in momentum, combined with bed expansion, results in a significant increase in torque. This indicates that, in contrast to low speeds, the medium faces greater difficulty in rearranging itself due to more frequent passages of the paddles through the powder bed. This is particularly true for high filling ratios as the bed dilatancy is more important.

While agitating the powder in the C-lab mixer, aside from the transition of regimes that takes place at the surface and is characterised by the Froude number, an immersed flow area can be observed. Fig. 10 shows both the flow that arises at the surface, which is essentially described by the Froude number, and the flow dynamics within the immersed region, which can be depicted through the velocity gradient from both side of a rotating paddle. The velocity gradient takes place within shear bands, where immersed flows take place [19].

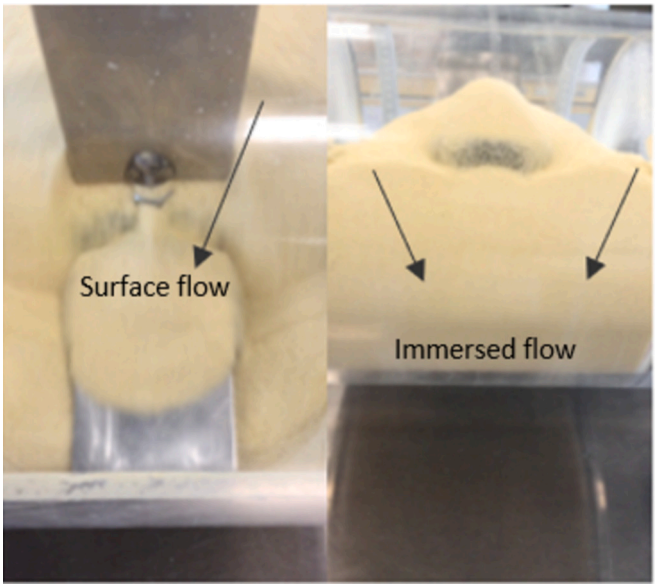

Fig. 10. Visualization of flow patterns in the C-lab mixer, depicting surface flow observations on top of paddles (left) and flow behaviour in the immersed area pushed by paddle motion (right).

3.2. Derivation of μ(I)-rheology through dimensional analysis

The Inertial Number I, often employed to describe dense flows, helps quantify the relative importance of particles inertia, arising from the applied shear, and interparticle friction, which opposes particle motion. However, while it provides insight into the predominance of inertia or friction within the granular media, it does not effectively measure the friction forces. Another parameter, the effective friction coefficient μ_{eff}, quantifies the local friction coefficient in the shear bands, providing a more detailed characterization of the dense flow dynamics. μ_{eff} is solely a function of I, which makes it a local law, referred to as μ(I)-rheology, describing the dense flow in the shear bands.

In order to apply the μ(I)-rheology in the C-lab mixer, a dimensional analysis was carried out through the Buckingham-Pi theorem. It states that a system that is represented by a number n of physical variables V_i measured by p fundamental dimensions can be described by a function between $n - p$ dimensionless numbers π_i, in a plane shear geometry that can be described by five key variables illustrated in Fig. 11.a:

- The mean particle diameter d (m) of particles in the sliding region.
- The particle density ρ_p (kg. m^{-3}).
- The normal stress σ (Pa) applied on the flowing region of height h_W.
- The shear stress τ (Pa), corresponding to the tangential force applied by moving wall on the flowing powder region.
- The shear rate $\dot{\gamma}$ (s^{-1}) representing the rate within the flowing region, at which layers of particles slide past each other due to the translation of the wall.

By analogy with the plane shear configuration, as shown in Fig. 11.b, and considering the C-lab mixer as a semi-confined system, the variables are henceforth defined as follows:

- The mean particle diameter d (m) of particles in the shear bands.
- The particle density ρ_p (kg. m^{-3}).

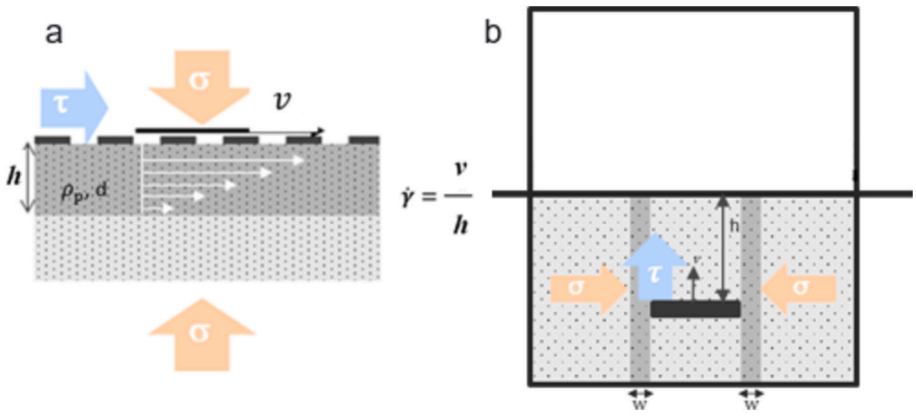

Fig. 11. Definition of key parameters for dimensional analysis within a shear plane geometry (a) and their analogy in the C-lab mixer (b): The shear stress τ, The normal stress σ, The shear rate γ, The paddle linear speed V and the powder bed height h.

- The normal stress σ (Pa) applied on the shear bands from both sides of the paddle.
- The shear stress τ (Pa), corresponding to the tangential force applied by the paddle on the powder.
- The shear rate $\dot{\gamma}$ (s^{-1}) representing the rate at which layers of particles slide past each other due the mechanical agitation within the shear band.

Table 2 summarizes the fundamental dimensions p of the five cited variables, which consists in length [L], mass [M], and time [T]. Thus, the system, defined by these five variables that are measured by three fundamental dimensions, can be represented by two independent dimensionless numbers: the effective friction coefficient μ_{eff} and the inertial number I.

The effective friction coefficient μ_{eff} is the ratio of the shear stress τ to the normal stress σ. The shear stress is defined as the tangential force F per unit surface area. The forces acting on the paddle are illustrated in Fig. 12.a. In this work, the shear stress is assumed to be uniform following the trajectory of the paddle. Additionally, the torque used for calculation is time-averaged over a two-minute agitation during the stationary regime. By definition, the torque is the product of force (F) and the perpendicular distance, which is the paddle length (L_p) considered to be equal to the radius R of cylinder given the small gap.

$$\tau = \frac{F}{S} = \frac{T}{SL_p} \tag{8}$$

Where S represents the friction surface (m^2) and L_p the paddle length (m). To base calculations consistently on time-averaged torque T, S is assumed to be equal to the whole filled cross-section area A_f described in Fig. 12. Additionally, the sheared surface is assumed to remain constant regardless of whether the powder is at rest or in motion. Given the existence of two shear bands on either side of the paddle, the friction surface is deemed to be twice the cross-sectional area. Fig. 12.b shows how the parameters are defined for the cylinder and the surface assumption made. The surface of friction calculated following (Eq. (9)):

$$S = 2 \times A_f = f \times 2 \times \pi^* R^2 \tag{9}$$

Table 2
Fundamental dimensions p of physical variables Vi describing the system.

V_i	Units	p
h	m	[L]
V_w	m. s^{-1}	[L. T^{-1}]
σ	Pa	[M·L $^{-1}$·T $^{-2}$]
τ	Pa	[M·L $^{-1}$·T^{-2}]
$\dot{\gamma}$	s^{-1}	[T^{-1}]

f is the volumetric filling ratio representing the volume occupied by the powder.

Since wall effects are neglected and the powder bed depth remains below the Janssen threshold, the normal stress σ applied on the shear bands is considered equal to the hydrostatic pressure P [29,34,35]. Moreover, the dynamic pressure has been deliberately excluded from these calculations, as particle interactions in dense flows are primarily governed by contact forces, likely minimizing the impact of dynamic pressure. Additionally, this study focuses on the stationary regime. Thus, the hydrostatic pressure P is calculated as:

$$\sigma = P = \rho_b g \overline{h_x} \tag{10}$$

ρ_b is the powder bulk density (kg.m^{-3}), g the gravitational acceleration (m.s^{-2}) and $\overline{h_x}$ is the average height of the powder bed (m), which is calculated differently depending on whether the powder bed is less than, equal to, or greater than the radius of the cylinder, as illustrated in Fig. 13. Depending on its position, a paddle may be fully, partially, or not at all immersed in the powder bed. Therefore, the average height $\overline{h_x}$ corresponds to the average variation of the powder bed height as the paddle rotates, with α representing the angle corresponding to the paddle's position relative to the powder bed surface. In the case where the mixer is filled up to the shaft axis, i.e., the maximum powder bed height H, corresponding to the paddle position when $\alpha = -\frac{\pi}{2}$, equals the radius of the mixer R and the length of the paddle L_p. Therefore, the average powder bed height is denoted h_1. Then, if the mixer is filled above the shaft axis, $\overline{h_x}$ becomes $h_{\frac{H}{R}>1}$. If it is filled below the axis, it will be denoted $h_{\frac{H}{R}<1}$.

To calculate the average height, the sine function in triangles is used to derive the powder bed height $h(\alpha)$ in front of the paddle as a function of its position α. The angle-averaged height $\overline{h_x}$ is then determined using the Mean Value Theorem by integrating $h(\alpha)$ from α_0, which is the first intersection of the paddle with the powder bed, to the angle where the paddle is fully out of the powder bed. The details of calculations are provided in Appendix.

The average height $\overline{h_x}$ of the powder bed for a filling ratio H/R equal to 1 ($x = 1$), which is the simplest scenario, is equal to:

$$\overline{h_1} = \frac{2R}{\pi} \tag{11}$$

For filling ratios smaller than 1:

$$\overline{h_{\frac{H}{R}<1}} = \frac{R}{\frac{\pi}{2} - \alpha_0} cos\alpha_0 - \mathrm{R}.sin\alpha_0 \tag{12}$$

With $\alpha_0 = sin^{-1}\left(1 - \frac{h}{R}\right)$.

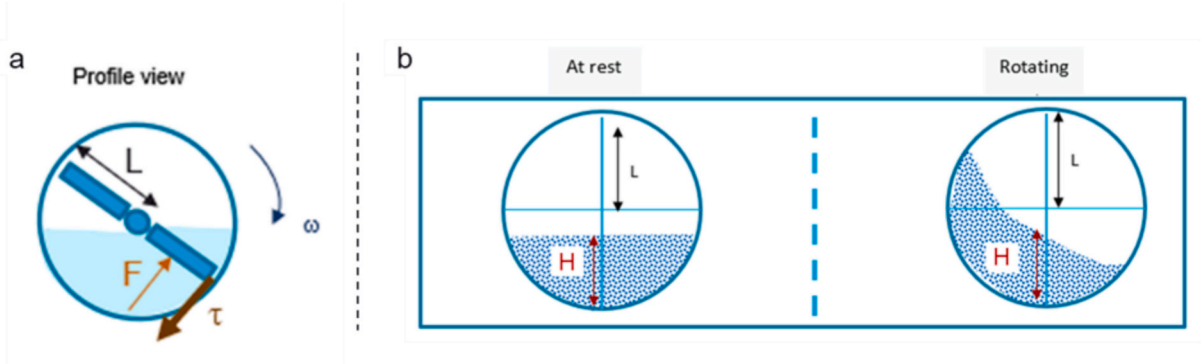

Fig. 12. Cross-sectional schematic of the C-lab mixer illustrating the shear and normal forces applied on the paddle (a) and the assumption on the friction surface during agitation (b).

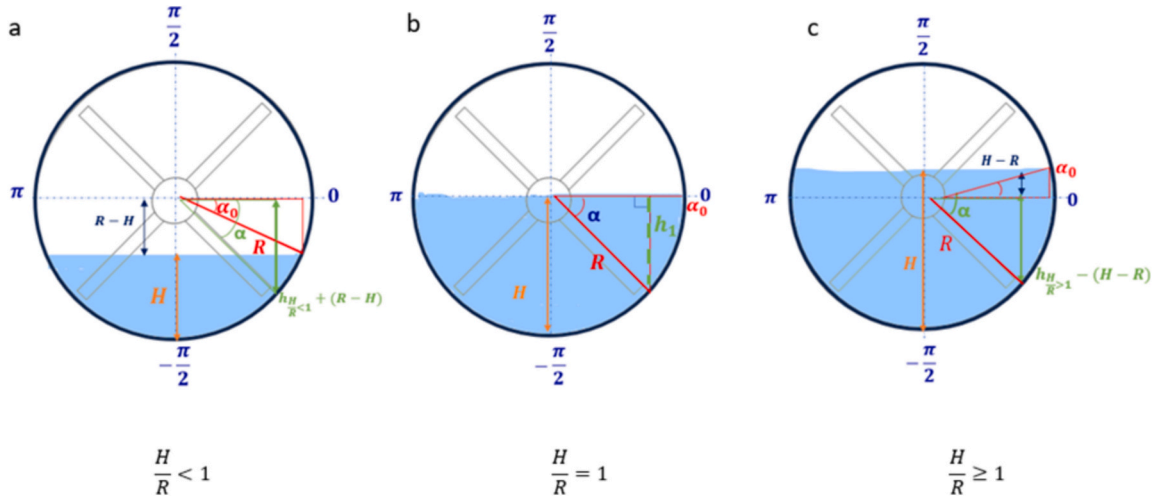

Fig. 13. Cross-sectional diagram illustrating three scenarios based on mixer filling. a. Filling below shaft axis $h_{H/R<1}$, b. filling up to the shaft axis h_1 and c. Filling above shaft axis $h_{H/R>1}$.

For filling ratios greater than 1:

$$\overline{h_{\frac{H}{R}\geq 1}} = \frac{R}{\frac{\pi}{2} - \alpha_0}(1 + sin\alpha_0) \tag{13}$$

With $\alpha_0 = sin^{-1}\left(\frac{h}{R} - 1\right)$.

Thus, according to (Eq. (9)) and above, the effective friction coefficient can be calculated as:

$$\mu_{eff} = \frac{\tau}{\sigma} = \frac{T}{\rho_b g \overline{h_x} SL} \tag{14}$$

On the other hand, the inertial number I as defined in the literature is calculated as follows:

$$I = \frac{\dot{\gamma} d}{\sqrt{P/\rho_p}} \tag{15}$$

Where the shear rate $\dot{\gamma}$ is the ratio of the linear speed of the paddle V_P to the width of the shear band given in (Eq. (7)). The inertial number in our study is then calculated using below:

$$I = \frac{\omega L_p}{k\sqrt{(\rho_b/\rho_p) g \overline{h_x}}} = \frac{\omega L_p}{k\sqrt{\Phi g \overline{h_x}}} \tag{16}$$

Φ, is assumed to be equal to the maximum packing fraction given in Table 1.

It is worth noting that he inertial number I, as defined in our study, is reminiscent of the Froude number Fr which describes flows appearing at the surface of a powder bed during mechanical agitation. I and Fr are related through the following, which is a combination of (Eq. (3)) and (Eq. (16)):

$$I = \frac{1}{k}\sqrt{\frac{FrL_p}{\Phi \overline{h_x}}} \tag{17}$$

Consequently, $Fr(I)$ relationship adheres perfectly to a squared power law as follows:

$$Fr = a.I^2 \tag{18}$$

Accordingly, the proportionality constant a can be expressed by (Eq. (19)) as L and R are considered equivalent in this work. a is a function of the shear band width, the packing of the powder bed and the filling ratio. Table 3 shows values of a corresponding to the present case.

Table 3
Values of proportionality constant a calculated using (Eq. (19)) across four HR for semolina and couscous.

Filling ratio	a - semolina	a - couscous
0.5	158	173
0.75	237	258
1	302	338
1.25	363	406

$$a = k^2.\Phi.\frac{\overline{h_x}}{L} \approx k^2.\Phi.\frac{\overline{h_x}}{R} \quad (19)$$

The Froude number *Fr* has always played a crucial role in describing flows within mixers with rotating effect. Its significance extends beyond industrial applications to academic research. However, it was found that relying solely on *Fr* may not provide a comprehensive understanding of powder behaviour during convective mixing, let alone accurately predict scale-up process. While *Fr* has been correlated with other dimensionless numbers, such as the power number N_p or the Newton number N_e, the integration of particle interactions and material properties has often been conducted without fully accounting for their specific characteristics.

Furthermore, during agitation, *Fr* describes the overall behaviour of the powder at the surface. However, the paddle—induced dense flows were shown to arise within shear bands from both sides of the moving paddles. Therefore, the μ(I)-rheology, which describes dense flows is more adequate to understand and then predict flow behaviour of free-flowing powders in convective mixers.

Having defined the two dimensionless numbers that compose the μ(I)-rheology, this empirical framework will be studied for semolina and couscous, similar powders of different particle size.

3.3. μ(I)-rheology assessment in the C-lab mixer

3.3.1. Global observation of dense regime

The evolution of μ_{eff} as a function of I for the agitation of semolina and couscous in the C-lab mixer for four filling ratios and twelve angular speeds is illustrated Fig. 14.

For both powders, the initial observation indicates that the values of I fall within the dense regime range according to the limits set by *Da* Cruz $[10^{-2}; 0.2]$. Additionally, the evolution of μ_{eff} with I exhibits a similar profile to that observed in the work of *Da* Cruz et al., in plane shear configuration. However, it is noteworthy that these limits are still vague in literature, as the dense regime ranges from 10^{-3} to 10^{-1} according to Chevoir et al., [23,24]. However, in the work of GDR MiDi, the collisional regime was characterised by an S-shaped curve, with μ_{eff} reaching saturation and then slightly decreasing. This trend is not observed in our study. Therefore, the limits to be considered in this work are those given by *Da* Cruz. Nevertheless, the uncertainty surrounding these limits, along with our data's close proximity to the quasi-static and collisional regime boundaries, raises doubts regarding the interpretation of extreme data points. Yet, this is not problematic as mixing equipment in industrial conditions seldom, if ever, operates within such shear rate ranges—either very low or very high.

3.3.2. Shear rate impact on μ(I)-rheology

The same pattern is observed for both powders. In the left-hand part of semolina and couscous charts illustrated in Fig. 14, μ_{eff} remains relatively constant, indicating that the powder flow is shear-independent and particle interactions are primarily due to friction forces. This behaviour can be attributed to the resistance of particles to flow in the shear band, where the shear rate is relatively weak. Consequently, particles around the paddle have time to rearrange themselves and return to their initial state. The force network within the shear band is important, but the shear rate is high enough to maintain a liquid-like flow. Therefore, the flow is considered insensitive to shear rate variations during this first phase of the dense regime.

However, at a certain critical value of inertial number that will be referred to as I_c, μ_{eff} starts increasing significantly with I. This critical value I_c marks the threshold above which the particles, still within the dense regime, are no longer able to return to their initial rearrangement, causing the powder bed to expand. Consequently, the interparticle friction in the shear bands becomes strongly influenced by variations in shear rate, primarily due to instantaneous collisions between particles.

In the first phase of the dense regime, where frictional forces dominate, the flow is termed "frictional dense flow." As the system approaches the critical inertial number I_c and moves past into the second phase, the flow behaviour transitions into what is termed "pre-collisional flow." This phase precedes the transition to the collisional regime and is characterised by significant interparticle collisions that dominate the flow dynamics. Fig. 15 illustrates the differentiation between these two phases for semolina at a filling ratio of $\frac{H}{R} = 1$.

The observed pattern remains consistent across approximately all tested filling ratios for both powders. Moreover, μ_{eff} demonstrates equivalent values for both powders in the frictional dense regime, which

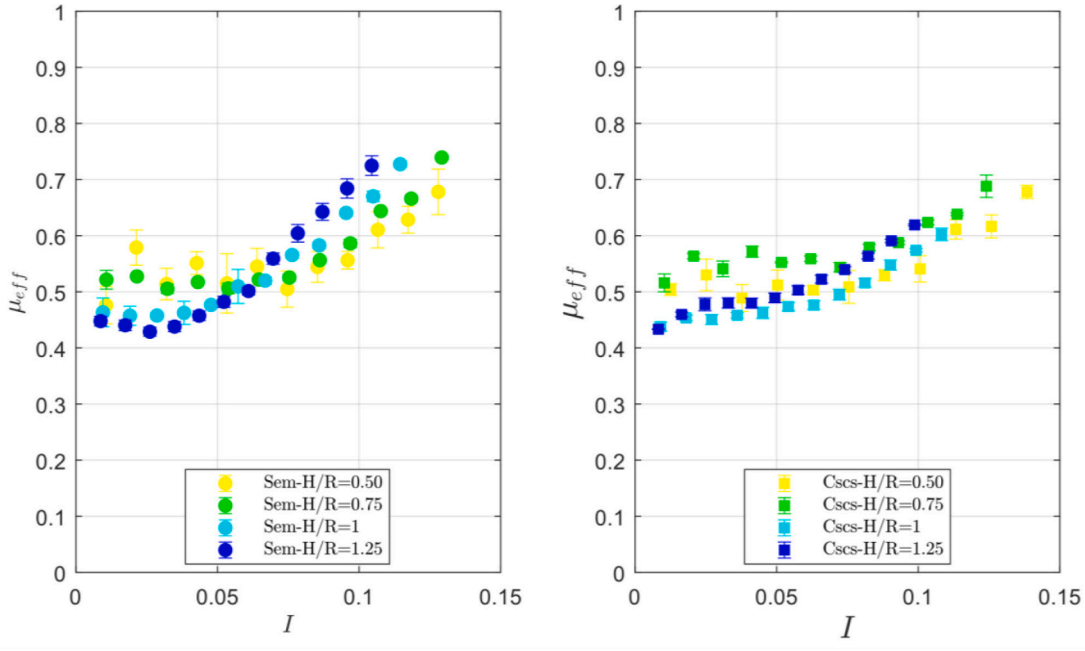

Fig. 14. (*I*)-*rheology* describing paddle-induced flows of semolina (●), couscous (■) in the C-lab mixer showing a dense flow regime and evidencing the existence of a transition in flow behaviour for four filling ratios.

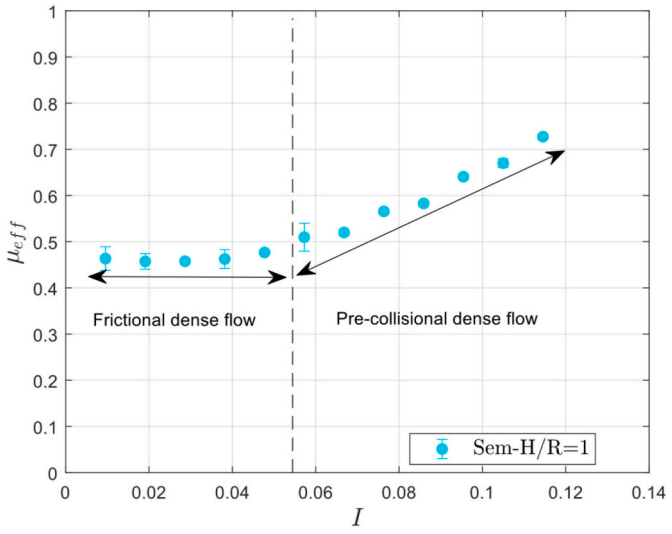

Fig. 15. Representation of the two observed flow behaviour in the μ(I)-rheology in the C-lab mixer with semolina for $H/R = 1$: frictional shear-independent and pre-collisional shear-dependent dense flows.

means that it seems independent of particle size. In the pre-collisional dense regime, it becomes smaller for couscous than for semolina. This change begins within the transition zone, as inertial forces start to dominate the frictional forces, as depicted in Fig. 16.

In the frictional dense regime, no difference can be observed between both particle types. Conversely, in the pre-collisional dense regime, semolina particles experience more collisions, as these are more numerous in a unit of volume than couscous particles. As a consequence, μ_{eff} is greater for semolina.

The pattern observed has then been fitted by Hatano's equation (2). Fig. 17 shows an example of least-square fit obtained with semolina for a linear filling ratio $\frac{H}{R} = 1$, which corresponds to 50 % of volumetric filling ratio (f). Hatano's equation demonstrates a good fit in this case, validating the presence of two distinct regimes within the dense flow itself with a transition observed around an I_c value of 0.05.

The fitting equation of μ(I)-rheology shows a coefficient of correlation NRMSE (Normalised Root Mean Squared Error) of 2,8 %. This translates to an average difference between the predicted and actual values of approximately 3 % of the total range of the data. This suggests

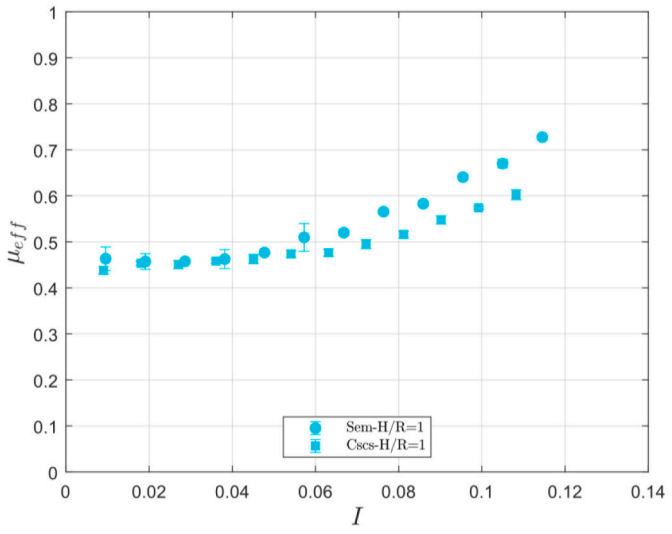

Fig. 16. Comparison of μ(I)-rheology of semolina (●) and couscous (■) in the C-lab mixer at $H/R = 1$.

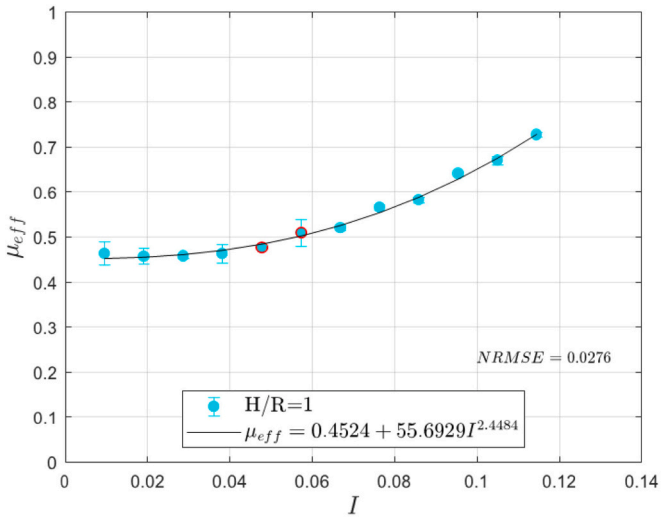

Fig. 17. Fitting of μ(I)-rheology of semolina for H/R = 1 by Hatano's equation, showing the threshold interval I_c (outlined in red) around which the transition between frictional and pre-collisional regimes appears. (For interpretation of the references to colour in this figure legend, the reader is referred to the web version of this article.)

a relatively small deviation between the model's predictions and the actual observations. Therefore, this law is considered to adequately fit the developed experimental model under these conditions. The different components of this relationship are:

- The minimum dynamic friction coefficient μ_0, which corresponds to the interparticle friction in a dynamic state at very low inertial numbers in the frictional dense regime, is equal to 0.45,
- The pre-exponential factor b describing the magnitude of increase of μ_{eff} with respect to I, might be attributed to the response of the particles in the shear bands to the shear rate. b is 55.69 for $\frac{H}{R} = 1$,
- The exponent n describing the nature of the change of μ_{eff} with respect to I, implies an accelerating relationship in this case as $n = 2.45$ $(n > 1)$.

Furthermore, it is important to underline the observed disparity in the values of μ_{eff} for high and low filling ratios as depicted in Fig. 14. Therefore, it is interesting to assess Hatano's law for both semolina and couscous across the tested filling ratios.

3.3.3. *Application of Hatano's law on the developed μ(I)-rheology*

Experiments were conducted at four filling ratios, both below and above the shaft axis. For $\frac{H}{R} < 1$, the powder bed is considered shallow, whereas for $\frac{H}{R} \geq 1$, it is considered deep. Fig. 18 shows the data for $\frac{H}{R} < 1$ and $\frac{H}{R} \geq 1$, plotted separately for couscous and semolina, with the transition zone, illustrated by dashed lines. The transition zone varies with varying filling ratios. For $\frac{H}{R} < 1$, I_c ranges between 0.07 and 0.09, while it ranges from 0.05 to 0.07 for $\frac{H}{R} \geq 1$. These findings highlight that I governs the transition from one regime to another by simply increasing the shear rate or decreasing the pressure, which was evidenced by GDR MiDi [14].

The sixth point of every $\mu_{eff}(I)$, corresponding to a Froude number $Fr = 1$, falls within the transition zone for $\frac{H}{R} \geq 1$, but lies before reaching it for $\frac{H}{R} < 1$. This proves that Fr does not govern the transition between the two observed behaviours in the dense regime. As the Froude number is designed to characterize flows at the surface rather than within immersed areas, this finding highlights the importance of considering μ(I)-rheology for paddle-induced flows.

The partition between the $\mu(I)$ law based on the filling ratio may

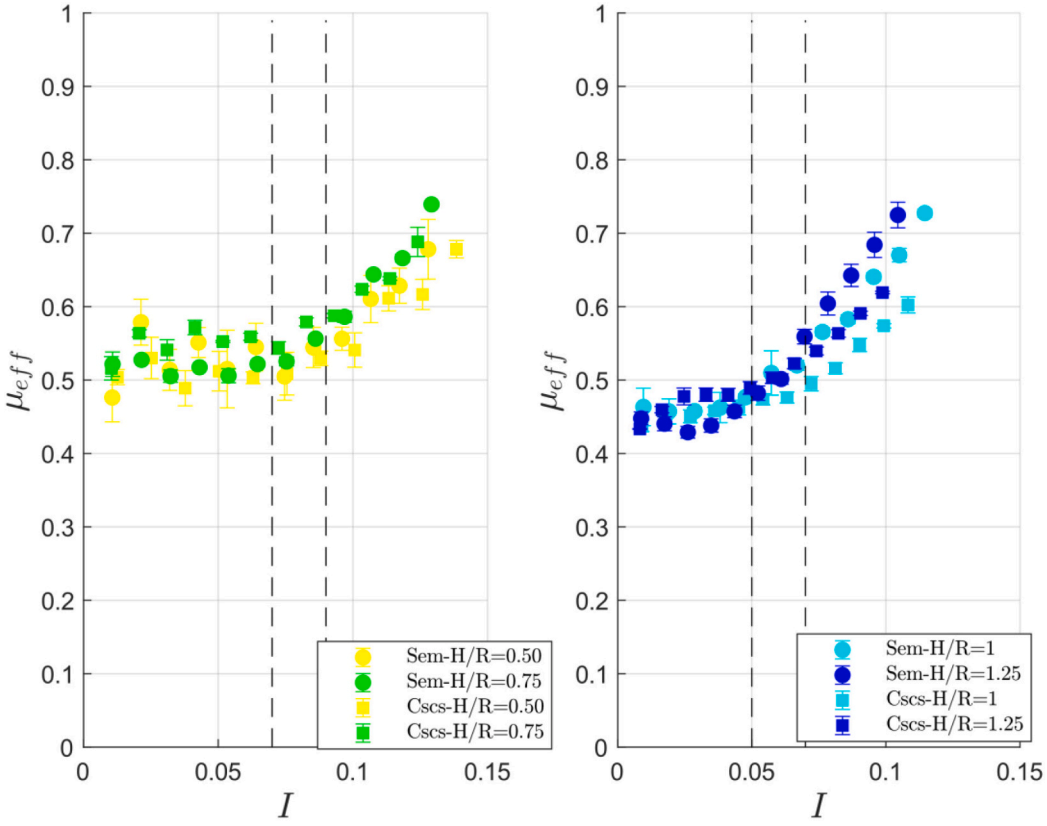

Fig. 18. Discrepancy of μ(I)-rheology of semolina (●) and couscous (■) in the C-lab mixer between low filling ratios (left) and high filling ratios (right) with the transition zone delineated by dashed lines.

result from the different behaviour of the powder during agitation. During experiments, it was observed that at low filling ratios (0.5 and 0.75), the powder in the middle of the tank is emptied due to the movement of the paddles. This phenomenon becomes more pronounced at higher speeds, corresponding to the cataracting regime according to the Froude number *Fr* and to pre-collisional regime according to the inertial number *I*. Our study, founded on immersed flows that take place when the powder is mechanically agitated, might be challenged at low filling ratios where the mixer is sparsely filled with powder. This is particularly true regarding the assumption of hydrostatic pressure being considered as the normal stress.

The obtained fitting parameters for semolina and couscous are summarised in Table 4. Consistently, the values of the parameters in these equations support the observed partition between the μ(I) – rheology at $\frac{H}{R} < 1$ and $\frac{H}{R} \geq 1$.

For both semolina and couscous, μ_0 and n exhibited a consistent trend, showing approximately the same values, with two distinct classes, as depicted in Fig. 19.

Table 4
Parameters of Hatano's equation applied to μ(I)-rheology of semolina and couscous.

Filling ratios		H/R = 0.5	H/R = 0.75	H/R = 1	H/R = 1.25
μ_0	Semolina	0.52	0.51	0.45	0.43
	Couscous	0.51	0.55	0.45	0.45
b	Semolina	3298.30	799.08	55.69	59.39
	Couscous	500.29	604.81	70.69	17.03
n	Semolina	4.84	3.98	2.45	2.32
	Couscous	4.10	4.01	2.74	2.00
NRMSE	Semolina	0.13	0.04	0.03	0.04
	Couscous	0.08	0.08	0.03	0.04

- Class I: Powder behaviour significantly sensitive to shear rate. This category includes shallow powder beds ($\frac{H}{R} < 1$), where the movement of the paddles through the centre of the mixer's tank displaces the powder towards the sides of the tank. The average minimum friction coefficient is $\mu_0^* = 0.52$ (± 0.02). Additionally, the average exponent n^* is 4.23 (± 0.41) and the pre-exponential factor b significantly high, is showing a considerable discrepancy between H/R = 0.5 and H/R = 0.75 for semolina.
- Class II: Powder behaviour less sensitive to shear rate. Deep powder beds ($\frac{H}{R} \geq 1$) fall into this category, where particles pack together and transmit forces more robustly, making the flow less susceptible to changes with shear rate and increasing its tendency to shear band formation. Under these conditions, average μ_0^* is 0.44 (± 0.01) average n^* is 2.38 (± 0.3).

These observations imply that the flow within shallower powder beds is more sensitive to shear rate than in deeper beds. The higher normal stress applied to particles within shear bands at high filling ratios leads to more densely packed flow areas. These findings are consistent with Legoix's work [13], where the exponent of the employed power law was also found to be dependent on the filling ratio. Additionally, based on the *NRMSE*, which corresponds to the average difference between the predicted and actual values of μ_{eff} over the total range of the data, the fitting of μ(I)-rheology exhibited a better accuracy for deep beds (4 %) than for shallow beds (8 %). Nevertheless, both powders present a fairly good fit, as the NRMSE values are below 12 %, indicating a good prediction of the law relative to the experimental data.

The analysis of the experimental rheological law μ(I)-rheology obtained for semolina and couscous along with the fitting parameters of Hatano's law, suggest that the μ(I)-rheology, which describes the paddle-induced flow behaviour of powders, effectively accounts for the

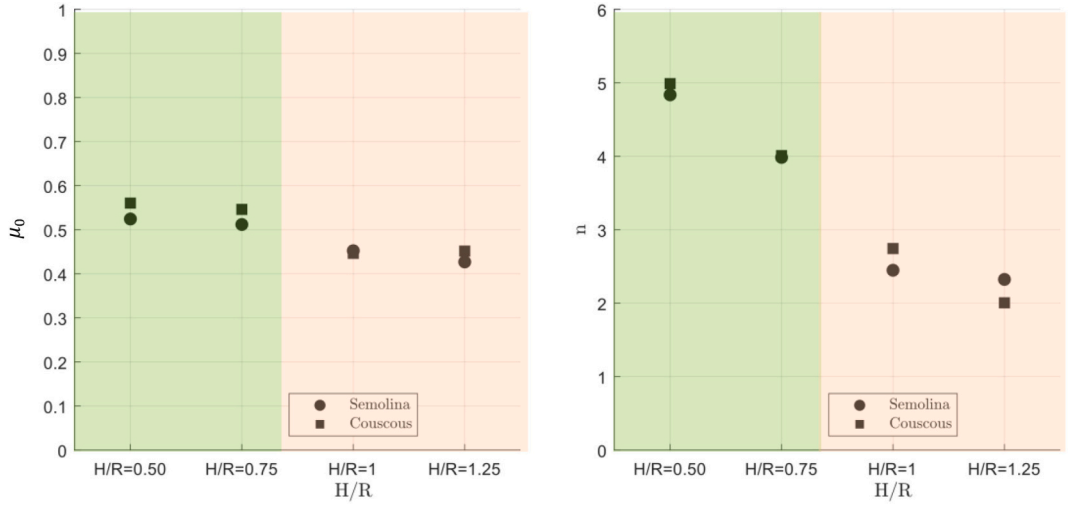

Fig. 19. Minimum effective friction coefficient μ_0 and exponent n obtained by fitting μ(I)-rheology of semolina (●) and couscous (■) by Hatano's equation showing the classification between shallow (Class I: green area) and deep (Class II: orange area) powder beds. (For interpretation of the references to colour in this figure legend, the reader is referred to the web version of this article.)

particle size difference when considering powders of the same particle shape. This is particularly obvious in the initial phase of the dense flow regime (Fig. 16), referred to as the frictional dense flow, where particles are closely packed, and shear bands are uniform from a flow and thickness perspective.

Given that b shows significant variation across different filling ratios, while μ_0 and n exhibit similar values within the same scenario (deep or shallow powder bed), a linearization of Hatano's law through (Eq. (20)) is performed. This involved fixing μ_0 and n to their average values for deep and shallow beds, respectively, and then observing the variation of b. The results of this fitting are illustrated in Fig. 20 and the obtained values of b are reported in Table 5.

Table 5
Pre-exponential factor b obtained by fixing μ_0* and n in Hatano's law for the μ(I)-rheology of semolina and couscous.

Filling ratios		H/R = 0.5	H/R = 0.75	H/R = 1	H/R = 1.25
b	Semolina	950.80	1271.27	50.12	62.56
	Couscous	595.58	1248.64	31.01	46.09

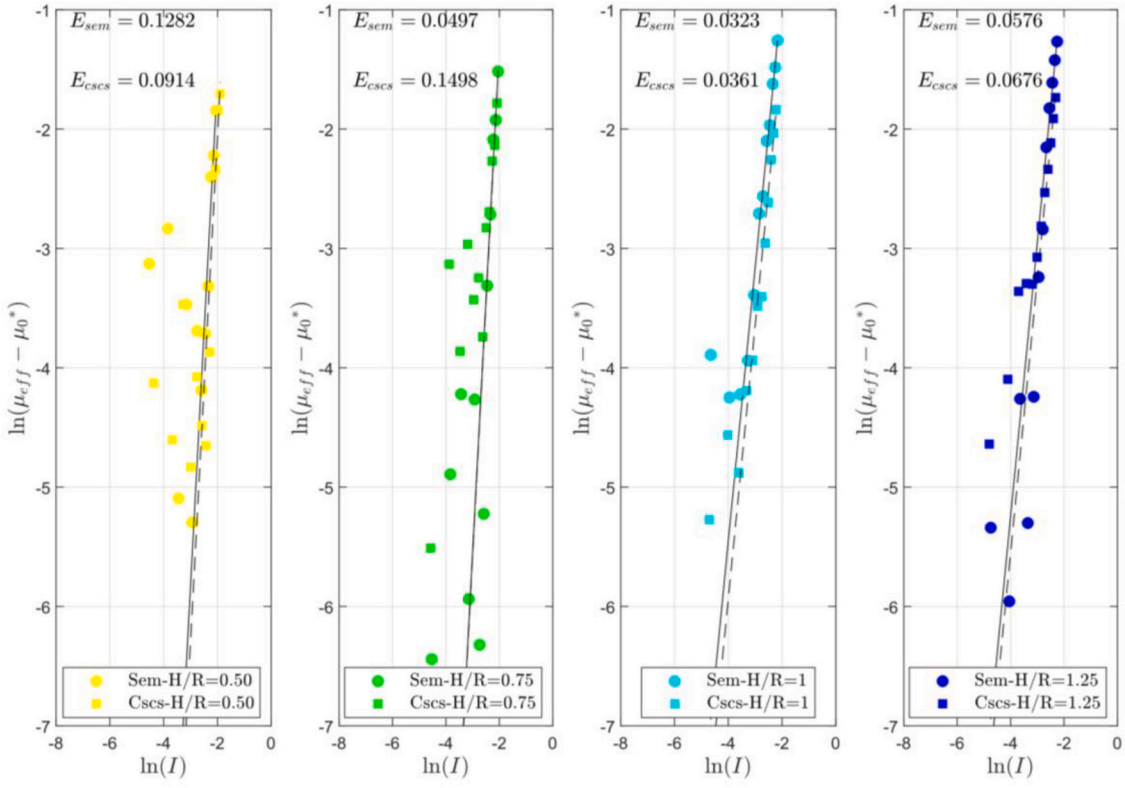

Fig. 20. Linearisation of μ(I)-rheology for semolina (●) and couscous (■) across four filling ratios H/R, along with linear fitting (solid for semolina and dashed for couscous) of the logarithmic variation of $(\mu_{eff} - \mu_0)$ as a function of the logarithm of I,with μ_0 and n fixed. The error metric NRMSE is referred to as E_{sem} and E_{cscs}.

$$ln\left(\mu_{\text{eff}} - \mu_0\right) = ln(\text{b}) + \text{n}.ln(\text{I}) \quad (20)$$

The pre-exponential factor *b*, capturing the magnitude of change in μ_{eff} with respect to *I*, is found to be consistently greater for semolina than couscous. This can be attributed to the semolina particles, three times smaller, being more sensitive to the shear rate change, although both powders exhibit similar behaviour when the shear rate tends to 0 (μ_0). The *NRMSE* obtained for all μ(I)-rheology data, except for semolina at $\frac{H}{R} = 0.5$ (13 %) and couscous at $\frac{H}{R} = 0.75$ (15 %), translates to a fair fitting of Hatano's equation to the developed empirical model. Overall, the *NRMSE* values, along with the visual scatter of data around the fitted line, show that Hatano's equation is less accurate for shallow powder beds ($\frac{H}{R} < 1$) in comparison to deep powder beds ($\frac{H}{R} \geq 1$).

Additionally, the higher NRMSE obtained for shallow powder beds supports the earlier observation that the μ(I)-rheology model better accounts for the behaviour of paddle-induced powder flow for deeper beds. At $\frac{H}{R} \geq 1$, the powder bed height is sufficient to form well-defined shear bands, which are critical for the dense flow regime that μ(I)-rheology is designed to describe. These shear bands facilitate a more consistent and predictable flow behaviour, making the model's assumptions and linear fitting more applicable and reliable. Conversely, at lower filling ratios $\frac{H}{R} < 1$, the powder bed is shallower, and the shear band formation may be affected with potential variations in local particle packing and rearrangement. Moreover, the shape of the powder bed is more subjected to change through mixing at low filling ratios [31]. These factors introduce more variability into the flow behaviour, leading to greater scatter in the data and a less accurate fit with the μ(I)-rheology under these conditions, as compared to agitation of deeper beds (Fig. 20).

The analysis of μ(I)-rheology of semolina and couscous across four filling ratios revealed that the developed model can be effectively described by Hatano's equation despite the significant difference in particle size. Therefore, a unified power law can be suggested to describe the flow behaviour of both semolina and couscous in the C-lab mixer. The fitting parameters correspond to the average values for deep and shallow beds, respectively. The fitting equations are described by (Eq. (21)) for $\frac{H}{R} < 1$ and (Eq. (22)) for $\frac{H}{R} \geq 1$. Subsequently, the linear representation following (Eq. (20)) is plotted in Fig. 21.

For shallow beds

$$\mu_{eff} = 0.52 + 1017I^{4.2} \quad (21)$$

For deep beds

$$\mu_{eff} = 0.44 + 47I^{2.4} \quad (22)$$

As expected for shallow bed, the linear representation of the data around a unique fitting line presents a greater scatter than for deep beds. The NRMSE decreases from 14 % at $\frac{H}{R} < 1$ to 9 % at $\frac{H}{R} \geq 1$. This reinforces the assumption that the μ(I)-rheology better predict flow behaviour at high filling ratios. However, comparatively larger deviations from the fitted line are observed at low shear rates. In the case of deep powder beds, the scatter is more pronounced for $ln(I) < -3$ ($I \approx 0.05$), whereas data roughly fall into a single master line at high shear rates ($I > 0.05$). For shallow powder beds, the scatter becomes less significant starting from $ln(I) > -2.5$ ($I \approx 0.08$), which also belongs to the defined threshold interval.

The value from which the unified law adequately fits the data belongs to the reported threshold interval where I_c is located where the transition zone takes places for both deep and shallow beds.

Powder mixing, where mechanical agitation is exerted on powder through paddle movement, essentially operates with deep powder beds

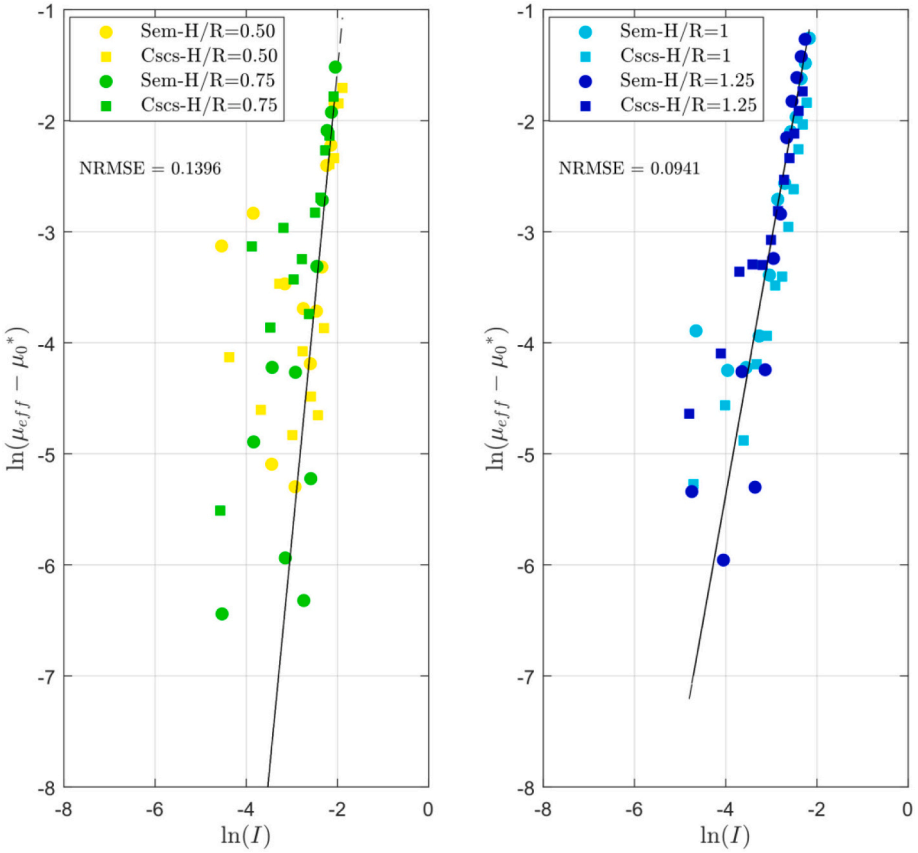

Fig. 21. Unified linear law to describe semolina's (●) and couscous' (■) μ(I)-rheology for H/*R* < 1 (on the left) and H/*R* ≥ 1 (on the right).

and at $Fr \approx 1$. This choice is due to the recommended balance between gravitational and inertial forces, allowing paddles to induce sufficient vertical movement and shear forces within the powder bed to overcome interparticle forces, such as friction or cohesion, thereby promoting effective mixing. Furthermore, operating at $Fr \approx 1$ avoids unnecessary energy consumption associated with very high paddle rotational speeds (thus high *Fr*), and minimizes the risk of particle degradation at high shear forces, while ensuring a good mixture homogeneity. According to (Eq. (20)), the Froude numbers *Fr* for deep filling ratios corresponding to $I = 0.05$ have been calculated and are reported in Table 6 for both powders. Notably, the transition to the pre-collisional regime starts at a significantly smaller *Fr*, indicating that the dense flow behaviour does not depend on the Froude number.

Focusing on the inertial number rather than the Froude number might offer additional opportunities for energy savings in industrial applications, while still achieving optimal mixing performance. This approach is supported by the observation that paddle-induced flows are primarily governed by interactions between the paddles and the shear bands, rather than by phenomena occurring at the surface.

Consequently, the application of the unified law of the developed rheological model μ(I)-rheology provides good insight into understanding in-depth paddle-induced flow behaviour during mechanical agitation, offering a reliable framework for modelling and optimizing powder mixing processes. Despite several assumptions, such as considering only hydrostatic pressure and the approximate estimation of shear band width, which may introduce a degree of approximation, the μ(I)-rheology-like law has demonstrated consistent results for two real powders, semolina and couscous, across various filling ratios.

4. Conclusions

Observing and understanding the physical phenomena during mixing processes have been the focus of many studies. However, the main emphasis has often been on surface flows, which have proven insufficient for accurately describing and predicting overall flow behaviour. This study provides a comprehensive analysis of powder rheology in a laboratory mixing set-up, concentrating on dense flow and the interaction between the agitation mobile (the paddle) and the powder bed.

The μ(I)-rheology framework offers a promising basis for understanding and modelling the flow behaviour of powders. In this framework, the development of μ(I)-rheology for mechanically agitated systems relies on key assumptions, such as considering the flow geometry as a plane shear rate and visually assessing the width of shear bands. These assumptions help overcome challenges in measuring complex powder parameters, such as particle velocities and the normal stress applied on the paddle by the powder bed, therefore establishing a practical model that can be easily applied.

The developed μ(I)-rheology seems to be an accurate descriptor for beds of any relative powder height, perhaps more so for deep powder beds than shallow ones. This can be attributed to modifications occurring within the powder beds during mechanical agitation. It also exhibited good predictive capabilities for flow behaviours of powders of similar particle shapes but different sizes. Even if the C-lab mixer used in this work for studying and implementing the μ(I)-rheology has a configuration distinct from that of an industrial mixer, paddle-powder interaction can be claimed to remain the same. In other words, the present work may serve directly for other mixers.

Future research should focus on using advanced techniques, such as high-speed cameras and Discrete Element Method (DEM) simulations, to gain deeper insights into powder flow dynamics. These techniques can help validate the μ(I)-rheology model across different powder types and industrial conditions. Additionally, investigating the influence of different mixer configurations, along with other free-flowing powders and agitation speeds will be essential for refining the model and enhancing its applicability in industrial processes. These studies are the focus of forthcoming research.

By addressing these limitations and exploring the outlined perspectives, the comprehension of powder flow behaviour in mixing processes can be notably advanced, paving the way for more efficient and dependable industrial operation. To the best of our knowledge, there remains an absence of a comprehensive rheological law that fully incorporates powder-specific characteristics to support accurate scaling up of mixing processes. Developing such a model could facilitate better predictions for diverse powders under varying operational conditions, providing valuable insights for process optimisation and design on an industrial scale.

Table 6
Froude numbers *Fr* calculated using Eq. (18) for $I = 0.05$ for semolina and couscous at HR = 1 and HR = 1.25.

$\frac{H}{R}$	*Fr*
1	0.75
1.25	0.90

Nomenclature

A_f	Filled cross-section area (m2)
AM	Agitation mobile (−)
CI%	Carr Index (−)
d_{10}	Mean diameter - First decile (μm)
d_{50}	Mean diameter - Median decile (μm)
d_{90}	Mean diameter - Last decile (μm)
f	volumetric filling ratio (−)
Fr	Froude number (−)
g	Gravitational acceleration $(m.s^{-2})$
h	Average powder bed height (m)
h_W	Flowing powder bed (m)
H	Maximum powder bed height (m)
I	Inertial number (−)
k	Number of particles (−)
L_p	Paddle (blade) length (m)
l_p	Paddle (blade) width (m)
NRMSE	Normalised Root Mean Squared Error (−)
P	Hydrostatic pressure (Pa)
R	Radius (tank or cell) (m)
S	Friction surface (m2)
T	Torque (N.m)
V_w	Linear speed $(m.\ s^{-1})$
W	Shear band width (m)
$\dot{\gamma}$	Shear rate (s^{-1})
μ_0	Minimum dynamic friction coefficient (−)
μ_{eff}	Effective friction coefficient (−)
ρ_b	Bulk density $(kg.m^{-3})$
ρ_p	Particle density $(kg.m^{-3})$
ρ_t	Tapped bulk density $(kg.m^{-3})$
φ	Bed compacity (−)
σ	Normal stress (Pa)
τ	Shear stress (Pa)
ω	Angular speed $(rad.s^{-1})$

CRediT authorship contribution statement

Hayfa Boussoffara: Writing – original draft, Investigation. **Cendrine Gatumel:** Validation, Supervision. **Blandine Malécot:** Validation, Supervision. **Maxime Viau:** Validation, Supervision. **Henri Berthiaux:** Writing – review & editing, Validation, Supervision.

Declaration of competing interest

None.

Appendix A. Appendix

Powder bed height calculation for three scenarios.
Case 1: H/R = 1 (The simplest scenario)
H: Powder height
$h_1(\alpha)$: Height at an angle α
$H_1 = \overline{h_1}$: Average height
L: Paddle length = R: Radius of the cross-section of the cylinder

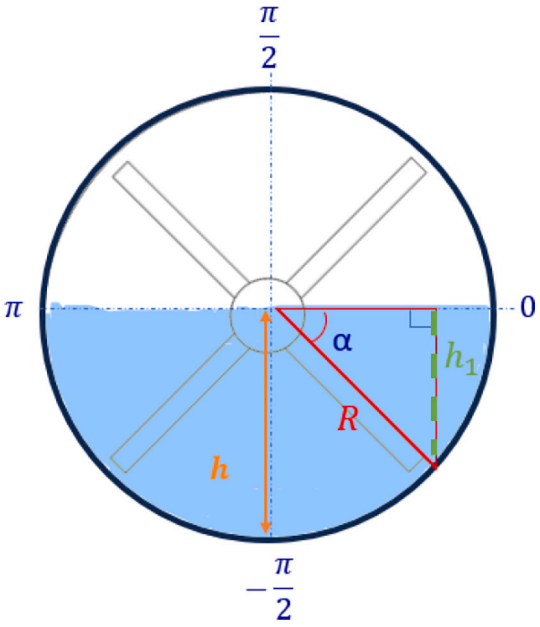

Fig A1. Filling ratio H/R = 1.

The law of Sines

$$sin\alpha = \frac{h_1(\alpha)}{R}$$

$$h_1(\alpha) = R.sin\alpha$$

The Mean Value Theorem

$$\overline{h_1} = \frac{1}{b-a}\int_a^b h_1(\alpha)d\alpha$$

In this specific case: $a = 0; b = \frac{\pi}{2}$

$$\overline{h_1} = \frac{1}{\frac{\pi}{2}-0}R\int_0^{\frac{\pi}{2}} sin\alpha d\alpha$$

$$\overline{h_1} = \frac{2R}{\pi}[-cos\alpha]_0^{\frac{\pi}{2}}$$

$$\overline{h_1} = \frac{2R}{\pi}$$

Case 2: H/R < 1

$h_{\frac{H}{R}<1}(\alpha)$: Height at an angle α

$H_{\frac{H}{R}<1} = \overline{h_{\frac{H}{R}<1}}$: Average height

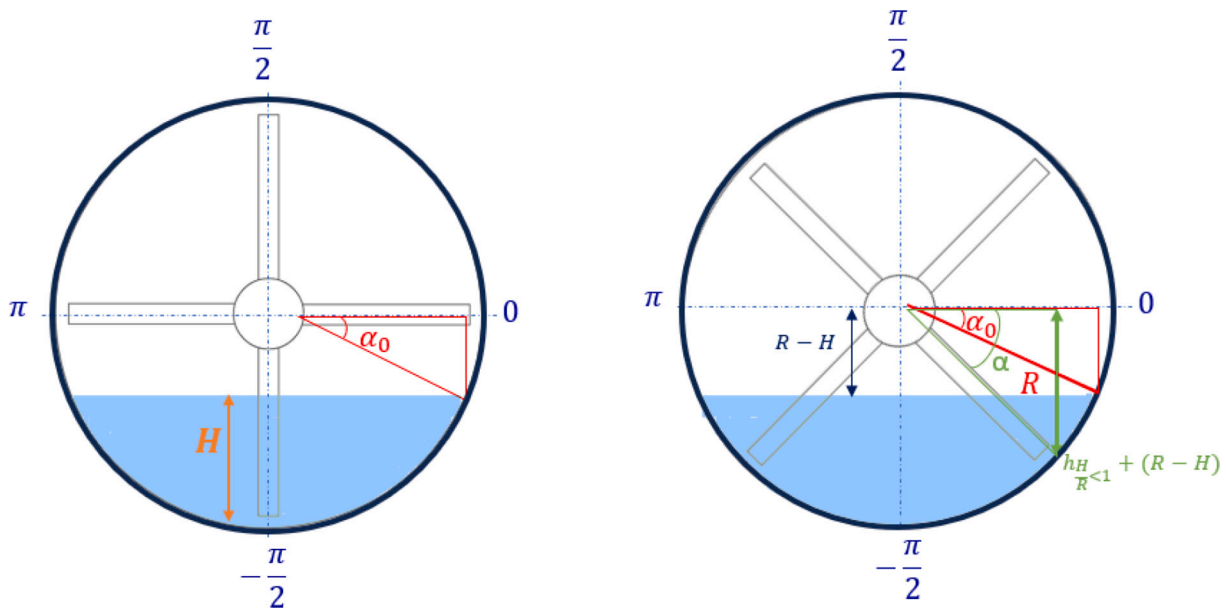

Fig A2. Filling ratio H/R < 1.

The Pythagorean theorem

$$sin\alpha = \frac{h_{\frac{H}{R}<1}(\alpha) + (R - H)}{R}$$

$$h_{\frac{H}{R}<1}(\alpha) = R.(sin\alpha) - R + H$$

The Mean Value Theorem

$$\overline{h_{\frac{H}{R}<1}} = \frac{1}{b-a}\int_a^b h_{\frac{H}{R}<1}(\alpha)d\alpha$$

In this case: $a = \alpha_0; b = \frac{\pi}{2}$

$$sin\alpha_0 = \frac{R-H}{R} = 1 - \frac{H}{R}; \alpha_0 = sin^{-1}\left(1 - \frac{H}{R}\right)$$

$$\overline{h_{\frac{H}{R}<1}} = \frac{1}{\frac{\pi}{2} - \alpha_0}\int_{\alpha_0}^{\frac{\pi}{2}} (R.(sin\alpha) - R + H)d\alpha$$

$$H_{\frac{H}{R}<1} = \frac{1}{\frac{\pi}{2} - \alpha_0}\left(R[-cos\alpha]_{\alpha_0}^{\frac{\pi}{2}} - (R-H)[\alpha]_{\alpha_0}^{\frac{\pi}{2}}\right)$$

$$\overline{h_{\frac{H}{R}<1}} = \frac{R}{\frac{\pi}{2} - \alpha_0}\left(cos\alpha_0 - sin\alpha_0 * \left(\frac{\pi}{2} - \alpha_0\right)\right)$$

$$\overline{h_{\frac{H}{R}<1}} = \frac{R}{\frac{\pi}{2} - \alpha_0}cos\alpha_0 - \mathrm{R}.sin\alpha_0$$

Case 3: H/*R* > 1

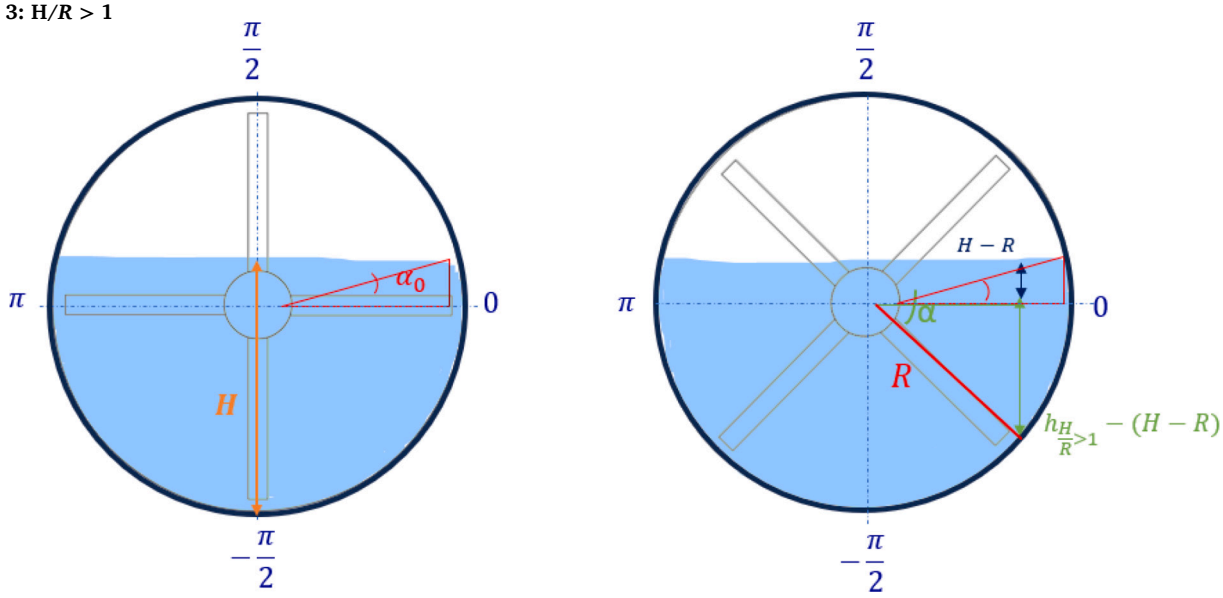

Fig. A3. Filling ratio H/L > 1.

$$h_{\frac{H}{R}>1}(\alpha) = h_1(\alpha) + \left(h_1(\alpha) - h_{\frac{H}{L}<1}(\alpha) \right)$$

$$sin\alpha_0 = \frac{H-R}{R}; \alpha_0 = sin^{-1}\left(\frac{H}{R} - 1\right)$$

Pour $\alpha \in [\alpha_0; 0]$ $h_{\frac{H}{R}>1}(\alpha) = Rsin\alpha$

Pour $\alpha \in [0; -\alpha_0]$ $h_{\frac{H}{R}>1}(\alpha) = 2Rsin(-\alpha)$

Pour $\alpha \in \left[-\alpha_0; -\frac{\pi}{2}\right]$ $h_{\frac{H}{R}>1}(\alpha) = Rsin(-\alpha) + Rsin\alpha_0$

The Mean Value Theorem

$$\overline{h_{\frac{H}{R}>1}} = -\frac{1}{\frac{\pi}{2}+\alpha_0}\left[\int_{\alpha_0}^{0} h_{\frac{H}{R}>1}(\alpha)d\alpha + \int_{0}^{-\alpha_0} h_{\frac{H}{R}>1}(\alpha)d\alpha + \int_{-\alpha_0}^{\frac{\pi}{2}} h_{\frac{H}{R}>1}(\alpha)d\alpha\right]$$

$$\overline{h_{\frac{H}{R}>1}} = -\frac{1}{\frac{\pi}{2}+\alpha_0}\left[\int_{\alpha_0}^{0} Rsin\alpha\, d\alpha + \int_{0}^{-\alpha_0} 2Rsin(-\alpha)\, d\alpha + \int_{-\alpha_0}^{\frac{\pi}{2}} Rsin(-\alpha) + Rsin\alpha_0 d\alpha\right]$$

$$\overline{h_{\frac{H}{R}>1}} = -\frac{1}{\frac{\pi}{2}+\alpha_0}\left[\frac{R}{\alpha_0}(cos\alpha_0 - 1) + \frac{R}{\alpha_0 - \frac{\pi}{2}}cos\alpha_0 + Rsin\alpha_0\right]$$

$$\overline{h_{\frac{H}{R}>1}} = -\frac{R}{\frac{\pi}{2}+\alpha_0}\left[\frac{(cos\alpha_0 - 1)}{\alpha_0} + \frac{cos\alpha_0}{\alpha_0 - \frac{\pi}{2}} + sin\alpha_0\right]$$

Data availability

Data will be made available on request.

References

[1] J.C. Williams, The mixing of dry powders, Powder Technol. 2 (1) (1968) 13–20, https://doi.org/10.1016/0032-5910(68)80028-2.

[2] H. Berthiaux, Mélange et homogénéisation des solides divisés, Ed. Techniques Ingénieur, 2002.

[3] G.V. Barbosa-Cánovas (Ed.), Food Powders: Physical Properties, Processing, and Functionality, Food engineering series, Kluwer Academic/Plenum Publishers, New York, 2005.

[4] J.M. Ottino, D.V. Khakhar, Mixing and segregation of granular materials, Annu. Rev. Fluid Mech. 32 (1) (2000) 55–91.

[5] M. Chen, et al., Caking of crystals: characterization, mechanisms and prevention, Powder Technol. 337 (Sep. 2018) 51–67, https://doi.org/10.1016/j.powtec.2017.04.052.

[6] D. Bagster, J. Bridgwater, The measurement of the force needed to move blades through a bed of cohesionless granules, Powder Technol. 1 (4) (1967) 189–198.

[7] D.F. Bagster, J. Bridgwater, The flow of granular material over a moving blade, Powder Technol. 3 (1) (Oct. 1969) 323–338, https://doi.org/10.1016/0032-5910(69)80104-X.

[8] M.S. Siraj, Single-blade convective powder mixing: the effect of the blade shape and angle, Powder Technol. 267 (Nov. 2014) 289–301, https://doi.org/10.1016/j.powtec.2014.07.024.

[9] S. Radl, D. Brandl, H. Heimburg, B.J. Glasser, J.G. Khinast, Flow and mixing of granular material over a single blade, Powder Technol. 226 (Aug. 2012) 199–212, https://doi.org/10.1016/j.powtec.2012.04.042.
[10] M.S. Siraj, Development of a mathematical relationship for prediction of mixing quality in industrial convective batch mixers, Part. Sci. Technol. 40 (4) (May 2022) 475–484, https://doi.org/10.1080/02726351.2021.1964657.
[11] L. Legoix, C. Gatumel, M. Milhé, H. Berthiaux, Characterizing powders in order to determine their flow behavior in a mixer: from small scale observations to macroscopic in-mixer rheology for powders of various flowabilities, Powder Technol. 322 (2017) 314–331, https://doi.org/10.1016/j.powtec.2017.07.075.
[12] L. Legoix, C. Gatumel, M. Milhé, H. Berthiaux, Analysis of powder flow and in-system rheology in a horizontal convective mixer with reclining blades, Part. Sci. Technol. 36 (8) (Nov. 2018) 955–966, https://doi.org/10.1080/02726351.2017.1331284.
[13] L. Legoix, Étude expérimentale et modélisation de mélangeurs convectifs: agitation de poudres de différentes coulabilités, 2017.
[14] G.D.R. MiDi, On dense granular flows, Eur. Phys. J. E: Soft Matter Biol. Phys. 14 (4) (Aug. 2004) 341–365, https://doi.org/10.1140/epje/i2003-10153-0.
[15] O. Pouliquen, F. Chevoir, Dense flows of dry granular material, C. R. Phys. 3 (2) (2002) 163–175.
[16] J. Lehuen, J.-Y. Delenne, A. Duri, T. Ruiz, Forces and flow induced by a moving intruder in a granular packing: coarse-graining and DEM simulations versus experiments, Granul. Matter 22 (4) (Nov. 2020) 78, https://doi.org/10.1007/s10035-020-01047-5.
[17] E. Andò, J. Desrues, P. Bésuelle, G. Viggiani, S. Hall, Un rêve devenu réalité: explorer une bande de cisaillement à l'échelle des grains, in: Proc. of the 18th ICSMGE, Paris, 2013.
[18] P. Guo, Critical length of force chains and shear band thickness in dense granular materials, Acta Geotech. 7 (1) (2012) 41–55, https://doi.org/10.1007/s11440-011-0154-3.
[19] C. Liu, Q. Sun, G.G. Zhou, Velocity profiles and energy fluctuations in simple shear granular flows, Particuology 27 (2016) 80–87.
[20] M. Mokni, Relations entre déformations en masse et déformations localisées dans les matériaux granulaires, Grenoble 1 (1992).
[21] P. Mort, et al., Dense granular flow — a collaborative study, Powder Technol. (2015) 14.
[22] A. Sadrekarimi, S.M. Olson, Shear band formation observed in ring shear tests on sandy soils, J. Geotech. Geoenviron. Eng. 136 (2) (2010) 366–375.
[23] F. Da Cruz, S. Emam, M. Prochnow, J.-N. Roux, F. Chevoir, Rheophysics of dense granular materials : discrete simulation of plane shear flows, Phys. Rev. E 72 (2) (Aug. 2005) 021309, https://doi.org/10.1103/PhysRevE.72.021309.
[24] F. Chevoir, J.-N. Roux, F. da Cruz, P.G. Rognon, G. Koval, Friction law in dense granular flows, Powder Technol. 190 (1–2) (Mar. 2009) 264–268, https://doi.org/10.1016/j.powtec.2008.04.061.
[25] B. Andreotti, Y. Forterre, O. Pouliquen, Granular Media: Between Fluid and Solid, Cambridge University Press, 2013.
[26] T. Hatano, Rheology of a dense granular material, in: Journal of Physics: Conference Series, IOP Publishing, 2007, p. 012015.
[27] R. Delannay, A. Valance, A. Mangeney, O. Roche, P. Richard, Granular and particle-laden flows: from laboratory experiments to field observations, J. Phys. D. Appl. Phys. 50 (5) (2017) 40, https://doi.org/10.1088/1361-6463/50/5/053001.
[28] T. Barker, J. Gray, Partial regularisation of the incompressible (I)-rheology for granular flow, J. Fluid Mech. 828 (2017) 5–32.
[29] F. Bouchut, J.M. Delgado-Sánchez, E.D. Fernández-Nieto, A. Mangeney, G. Narbona-Reina, A bed pressure correction of the friction term for depth-averaged granular flow models, Appl. Math. Model. 106 (2022) 627–658.
[30] L. Chupin, T. Dubois, M. Phan, O. Roche, Pressure-dependent threshold in a granular flow: numerical modeling and experimental validation, J. Non-Newtonian Fluid Mech. 291 (May 2021) 104529, https://doi.org/10.1016/j.jnnfm.2021.104529.
[31] V. Boonkanokwong, R.P. Frank, P. Valliappan, B. Remy, J.G. Khinast, B.J. Glasser, Flow of granular materials in a bladed mixer: effect of particle properties and process parameters on impeller torque and power consumption, Adv. Powder Technol. 29 (11) (Nov. 2018) 2733–2752, https://doi.org/10.1016/j.apt.2018.07.022.
[32] M.J. Khala, C. Hare, C.-Y. Wu, N. Venugopal, M.J. Murtagh, T. Freeman, Rheological response of granular materials under dynamic conditions, Powder Technol. 398 (Jan. 2022) 117074, https://doi.org/10.1016/j.powtec.2021.117074.
[33] K. Marikh, Mélange des poudres en continu: dynamique et modélisation', phdthesis, Institut National Polytechnique de Lorraine, 2003. Accessed: Apr. 15, 2024. [Online]. Available: https://hal.univ-lorraine.fr/tel-01750168.
[34] H.A. Janssen, Versuche uber getreidedruck in silozellen, Z. Ver. Deut. Ing. 39 (1895) 1045.
[35] D.-H. Nguyen, É. Azéma, P. Sornay, F. Radjai, Rheology of granular materials composed of crushable particles, Eur. Phys. J. E 41 (2018) 1–11.